

Re-examination of nuclear structure properties and shape co-existence of nuclei around $A \sim 70$

Jameel-Un Nabi¹, Tuncay Bayram², Mahmut Büyükata³, Asim Ullah^{4,1}, Anes Hayder² and Syeda Zainab Naqvi¹

¹*University of Wah, Quaid Avenue, Wah Cantt 47040, Punjab, Pakistan*

²*Department of Physics, Faculty of Science, Karadeniz Technical University, 61080, Trabzon, Türkiye*

³*Department of Physics, Faculty of Engineering and Natural Sciences, Kırıkkale University, 71450, Kırıkkale, Türkiye*

⁴*Department of Physics, University of Swabi, Swabi 23561, KP, Pakistan*

Abstract

We re-examine the nuclear structure properties of waiting point nuclei around $A \sim 70$ using the interacting boson model-1 (IBM-1) and the relativistic mean field (RMF) model. Effective density-dependent meson-exchange functional (DD-ME2) and density-dependent point-coupling functional (DD-PC1) were used for the RMF calculations. We calculated the energy levels, the geometric shapes, binding and separation energies of nucleons and quadrupole deformation parameters (β_2). The shape co-existence phenomena in $A \sim 70$ nuclei (^{68}Se , ^{70}Se , ^{70}Br , ^{70}Kr , ^{72}Kr , ^{74}Kr , ^{74}Rb and ^{74}Sr) was later investigated. Spherical and deformed shapes of the selected waiting point nuclei were computed using the IBM-1 and RMF models, respectively. The proton-neutron quasiparticle random phase approximation (pn-QRPA) model was used to calculate β -decay properties (Gamow-Teller strength distributions, β -decay half-lives and branching ratios) of selected nuclei as a function of β_2 . The results revealed a significant variation in calculated half-lives and Gamow-Teller strength distributions as the shape parameter was changed. The β_2 computed via DD-ME2 functional resulted in half-lives in best agreement with the measured data.

Keywords: Gamow-Teller strength, IBM-1 model, Nuclear deformation, Nuclear

¹asimullah844@gmail.com

1. Introduction

After Rutherford discovered the atomic nucleus, many exciting questions arose in the beginning of nuclear physics pertaining to the fundamental nature of the nuclear force and the intricate dynamics governing the coexistence of protons and neutrons in a very compact nucleus. The geometric structure of the nucleus can provide information on the nature of the interactions between its constituents. The behavior of nuclear forces gives rise to intriguing phenomena, including shape co-existence. Low-lying 0^+ states in connection with 2^+ states above ground-state of even-even nuclei were deliberated much earlier [1, 2]. Collective behavior of nucleon forces was held responsible for the deformation of the nucleus. Shape co-existence refers to the existence of multiple closely spaced eigenstates with varying intrinsic deformation within a finite nuclear many-body quantum system [3]. The shape-coexistence phenomena in atomic nuclei is a remarkable aspect of nuclear structure and the finite many-body quantum system. Shape coexistence allows researchers to examine how diverse sources contribute to correlation energy within the same nucleus, namely the quadrupole degree of freedom [4]. Shape transition and shape co-existence play a crucial role in comprehending the properties of low-lying nuclear structures and characterizing neutron-deficient isotopes [5, 6]. The phenomenon of shape co-existence is a manifestation of two opposing forces within the atomic nuclei. Whereas closed (sub)shells produce a stabilizing effect, the residual interactions between the nucleons tend to break the spherical symmetry and favor nuclear deformation. The concept of shape co-existence [2] is observed in both light and heavy nuclei. Various reactions in the past (e.g., [7]) provided evidence of shape co-existence and recent years have witnessed an increased emphasis on experimental as well as theoretical investigations in this field.

Neutron-deficient isotopes in the lead region serve as well-established examples defending shape co-existence phenomenon in nuclei [3]. Studies (e.g., [8, 9]) have revealed that the decay characteristics of β -unstable nuclei can be influenced by the nuclear shape of the decaying nucleus. Investigations have systematically examined the Gamow-Teller (GT) strength distributions associated with the β^+ /EC-decay of neutron-deficient nuclei in the $A \sim 70$ mass range [10]. These studies utilized a deformed quasiparticle random-phase approximation (QRPA) approach, with a self-consistent Hartree-Fock (HF) mean field and Skyrme forces, to analyze the dependence of GT strength on nuclear deformation. Similar analyses

were later extended to stable fp -shell [11] and neutron-rich nuclei in the $A \sim 100$ mass region [12]. The influence of deformation on GT strength distributions has proven to be a powerful tool in determining nuclear shape in neutron-deficient Kr and Sr isotopes. This was achieved by comparing theoretical predictions with β -decay measurements [13].

The problem of shape co-existence becomes more complex for nuclei close to the $N = Z$ line due to the competition between neutron-proton and like-nucleon interactions, which is expected to influence the behavior of these nuclei significantly [14]. Previously, the calculations of the interacting boson model-1 (IBM-1) and the proton-neutron quasiparticle random phase approximation (pn-QRPA) were performed to investigate the nuclear structure properties of the waiting point (WP) nuclei along $N=Z$ chain around $A \sim 70$ mass region [15, 16] and ^{76}Se isotope in same region [17]. In the mass region $A \sim 70$, few nuclei are predicted to possess a prolate surface state for $N \approx Z \approx 38$ & 40 and an oblate surface state for $N \approx Z \approx 36$. Most of these nuclei are expected to showcase shape-mixing [4, 9, 18, 19, 20, 21, 22]. Consequently, numerous nuclear experiments have been conducted, and in some cases, strong predictions have been made regarding the prolate-oblate coexistence in this region. Neutron-deficient nuclei in the mass region $A \sim 70$ are involved in rapid-proton capture (rp) nucleosynthesis and exhibit varying shapes and structural changes. These are attributed to the large gap in the spectrum of single particle energies at different deformations, which results in a robust struggle between varying many-body configurations based on corresponding deformations [23]. The astrophysical significance of the long-lived nuclei like $^{68-70}\text{Se}$ and $^{72-74}\text{Kr}$ could be that the proton capture increase the reaction flow, thus reducing the timescale for the rp -process nucleosynthesis during the cooling phase. The β -decay properties of the low-lying states in neutron-deficient nuclei, bearing relevance to rp -process, are argued to influence their effective β -decay half-lives for high temperatures prevailing in X-ray bursts [24].

Nuclei in $A \sim 70$ region are more dynamic in terms of their structural configurations, with diverse shapes coexisting and transitioning more readily than in other regions with equal numbers of neutrons or protons. We selected eight nuclei (^{68}Se , ^{70}Se , ^{70}Br , ^{70}Kr , ^{72}Kr , ^{74}Kr , ^{74}Rb and ^{74}Sr) from this mass region for our investigation. The selected nuclei play crucial roles in the rp -process in astrophysical environments. They act as WP nuclei, influencing the reaction flow and nucleosynthesis calculations. The selected nuclei exhibit complex nuclear structures, including shape coexistence and collective properties, making them ideal candidates for studying the interplay of different nuclear shapes and configurations in the $A \sim 70$ region. Advanced experimental techniques, such as decay studies and

gamma-ray spectroscopy, enable researchers to investigate the decay properties and nuclear structure of the selected nuclei in detail. Not all nuclei in the $A \sim 70$ region are relevant to the rp -process or serve as WP nuclei. Only a subset of nuclei meet these criteria and were prioritized for the current study. We employ three different theoretical approaches in the current investigation: the IBM-1, the relativistic mean field (RMF) and pn-QRPA model. The IBM-1 and RMF models were used to calculate the nuclear structure properties. These include energy levels, geometric shapes, binding and separation energies of nucleons and quadrupole deformation parameters (β_2) of the selected nuclei. The deformation parameters were calculated by plotting the potential energy surfaces (PESs). Later, the pn-QRPA model was used to study the β -decay properties of selected nuclei as a function of the computed deformation parameters. It is noted that the β_2 values enter as an input parameter in the pn-QRPA calculation. Five different values of β_2 , computed from the IBM-1 and RMF models, were used as a free parameter in the pn-QRPA calculation. A sixth value of deformation parameter was adopted from the FRDM calculation [25]. The measured value of β_2 , wherever available, was taken from the National Nuclear Data Center [26].

The paper's structure is as follows: In Section 2, we briefly describe the theoretical framework employed in our calculations. Section 3 presents the outcomes and findings of the study. In Section 4, we provide a summary of our investigation along with some concluding remarks.

2. Nuclear Models

The necessary formalism of the three nuclear models, used in the current investigation, is described briefly in the succeeding subsections.

2.1. Interacting Boson Model-1 (IBM-1)

The IBM-1 model proves to be effective in describing the nuclear structure properties of even-even nuclei [27]. This algebraic model is constructed on the six-dimensional $U(6)$ unitary group which has three possible subgroups called as *dynamical symmetries*. These symmetries are indicated by $U(5)$, $SU(3)$ and $O(6)$. The value of energy ratio ($R_{4/2}$) of 4_1^+ to 2_1^+ levels in the ground state band can provide insight into the geometrical behavior of the nucleus. The characteristic energy ratio values for $SU(3)$, $U(5)$, and $O(6)$ symmetries are 3.33, 2.00, and 2.50 for axially deformed (oblate/prolate), spherical, and γ -unstable shapes, respectively.

The IBM-1 model describes a system of the s - and the d -bosons interactions with angular momenta $L=0$ and $L=2$, respectively. The model Hamiltonian can be written in the form of combinations of the s , s^\dagger , d , d^\dagger operators [27] of the s - and d -bosons. The Hamiltonian is also written in terms of Casimir operators of the dynamical symmetries. For the present application, the multipole form of Hamiltonian [28] was selected as

$$\hat{H} = \varepsilon \hat{n}_d + \kappa \hat{Q} \cdot \hat{Q} + \kappa' \hat{L} \cdot \hat{L}, \quad (1)$$

where \hat{n}_d , \hat{Q} , \hat{L} are the boson-number, quadrupole and angular momentum operators, respectively, defined in the form of combination of the operators s , s^\dagger , d , d^\dagger

$$\begin{aligned} \hat{n}_d &= \sqrt{5}[d^\dagger \times \tilde{d}]_0^{(0)}, \\ \hat{Q} &= [d^\dagger \times \tilde{s} + s^\dagger \times \tilde{d}]^{(2)} + \chi [d^\dagger \times \tilde{d}]^{(2)}, \\ \hat{L} &= \sqrt{10}[d^\dagger \times \tilde{d}]^{(1)}. \end{aligned} \quad (2)$$

The constants ε , κ , κ' in Eq. (1), and χ associated with the quadrupole operator \hat{Q} , serve as free parameters in the Hamiltonian. These parameters are adjustable and can be tuned to match the experimental data [26] to calculate the energy levels of a given nucleus. Besides energy level calculation, the geometric shape of nuclei can also be predicted by plotting the energy surface as a function of the deformation parameters. The PES as a function of β and γ , obtained from the model Hamiltonian (1) in the classical limit [29, 30], can be formulated as follows

$$\begin{aligned} V(\beta, \gamma) &= \varepsilon_d \frac{N\beta^2}{1+\beta^2} + \kappa' 6N \frac{\beta^2}{1+\beta^2} + \kappa \frac{N}{1+\beta^2} \\ &\times \left[5 + (1+\chi^2)\beta^2 + \frac{(N-1) \left(\frac{2\chi^2\beta^2}{7} - 4\sqrt{\frac{2}{7}}\chi\beta \cos 3\gamma + 4 \right) \beta^2}{1+\beta^2} \right], \end{aligned} \quad (3)$$

where N is number of the bosons. The ε , κ , κ' and χ are common parameters given as constants in Eqs. (1) - (2). The β and γ variables are called deformation parameters and are the same as introduced in the collective model of Bohr and Mottelson [31]. Both parameters (β and γ) are *zero* for spherical nuclei while $\beta \neq 0$, $\gamma = 0^\circ$, and 60° for prolate and oblate nuclei, respectively.

2.2. Relativistic Mean Field (RMF) Model

In RMF model, a nucleus is described as a system of Dirac nucleons coupled to exchange of various mesons such as isoscalar scalar σ meson, the isoscalar

vector ω meson, and the isovector vector ρ meson together with the electromagnetic field [32, 33, 34]. In addition, a treatment of nuclear matter and finite nuclei requires a medium dependence of effective mean-field interactions. This dependence can either be introduced by assuming an explicit density dependence for the meson-nucleon couplings or by including non-linear meson self-interaction terms in the phenomenological Lagrangian density [35]. One can find many approaches for the construction of successful phenomenological non-linear RMF interactions (i.e NL3, PK1, PK1R FSUGold). Later density-dependent versions of RMF model were introduced. The density dependence of the meson-nucleon vertex functions can be parameterized either from microscopic calculations of nuclear matter or adjusting data and empirical properties of finite nuclei. Meson exchange is the convenient effective nuclear interaction for the ground state and low-lying excited states of finite nuclei. However, exchange of heavy mesons is associated with the short distance dynamics which means that it cannot be resolved at low energies. Because of this reason, density-dependent point coupling version of RMF model was introduced. In this version, meson exchanges are replaced by the corresponding local four-point interactions between nucleons. More details and discussions of the versions of the RMF model can be found in Refs. [36, 37, 38, 39, 40, 41, 42, 43].

In the current investigation, we have used effective density-dependent meson-exchange functional, DD-ME2 [44] and density-dependent point-coupling functional, DD-PC1 [45] for RMF calculations. It should be noted that we have restricted ourselves to describing only the meson-exchange version of the RMF model in this subsection.

In the density-dependent meson-exchange framework of RMF model, the nucleus is defined as a set of Dirac nucleons interacting through the exchange of mesons, resulting in finite-range interactions [38]. The Lagrangian equation of the meson-exchange version of the model can be divided into three parts as follows

$$\mathcal{L} = \mathcal{L}_N + \mathcal{L}_m + \mathcal{L}_{int}, \quad (4)$$

where \mathcal{L}_N , \mathcal{L}_m and \mathcal{L}_{int} terms are related with free nucleon, fields of the free meson and electromagnetic fields, and meson-nucleon interactions, respectively [37, 40]. Open form of \mathcal{L}_N term is given by

$$\mathcal{L}_N = \bar{\Psi}(i\gamma_\mu \partial^\mu - m)\Psi, \quad (5)$$

where the Dirac spinors ($\bar{\Psi}$ and Ψ), m , and γ_μ represent the nucleon field, meson field, nucleon mass, and Dirac gamma matrices, sequentially. Lagrangian density

for the meson and electromagnetic fields (\mathcal{L}_m) is given as

$$\begin{aligned} \mathcal{L}_m = & \frac{1}{2} \partial_\mu \sigma \partial^\mu \sigma - \frac{1}{2} m_\sigma^2 \sigma^2 - \frac{1}{2} \Omega_{\mu\nu} \Omega^{\mu\nu} + \frac{1}{2} m_\omega^2 \omega_\mu \omega^\mu \\ & - \frac{1}{4} \vec{R}_{\mu\nu} \cdot \vec{R}^{\mu\nu} + \frac{1}{2} m_\rho^2 \vec{\rho}_\mu \cdot \vec{\rho}^\mu - \frac{1}{4} F_{\mu\nu} F^{\mu\nu}. \end{aligned} \quad (6)$$

This term includes the kinetic energy of the meson field, potential energies of the σ , ω and ρ mesons and the electromagnetic field. In Eq. (6), arrows represent isovectors and m_σ , m_ω and m_ρ are the mass of σ , ω and ρ mesons, respectively. Field tensors are given by the following equations

$$\begin{aligned} \Omega_{\mu\nu} &= \partial_\mu \omega_\nu - \partial_\nu \omega_\mu, \\ \vec{R}_{\mu\nu} &= \partial^\mu \vec{\rho}_\nu - \partial_\nu \vec{\rho}_\mu, \\ F_{\mu\nu} &= \partial_\mu A_\nu - \partial_\nu A_\mu. \end{aligned} \quad (7)$$

In Eq. (4), \mathcal{L}_{int} is the interaction term, which refers to the interaction between mesons and nucleons, given by

$$\begin{aligned} \mathcal{L}_{int} = & -g_\sigma \bar{\Psi} \Psi \sigma - g_\omega \bar{\Psi} \gamma^\mu \Psi \omega_\mu - \\ & g_\rho \bar{\Psi} \vec{\tau} \gamma^\mu \Psi \cdot \vec{\rho}_\mu - e \bar{\Psi} \gamma^\mu \Psi A_\mu, \end{aligned} \quad (8)$$

where the coupling constants of the σ , ω and ρ mesons are defined by g_σ , g_ω and g_ρ , sequentially [37, 39, 40, 41]

A Hamiltonian density of the static case can be calculated from the Lagrangian density. The total energy (E_{RMF}), which depends on the Dirac spinors and the meson fields, is obtained by integrating Eq. (4) over the r-space.

$$E_{RMF} [\Psi, \bar{\Psi}, \sigma, \omega^\mu, \vec{\rho}^\mu, A^\mu] = \int d^3r \mathcal{H}(\mathbf{r}). \quad (9)$$

The density-dependent meson-exchange model incorporates an explicit density dependence for the meson-nucleon vertices. To determine the properties of finite nuclei, the meson-nucleon vertex functions can be adjusted by tuning the parameters of the meson-nucleon couplings' density dependence [44].

In this paper, we have used effective density-dependent meson-exchange DD-ME2 and point-coupling DD-PC1 functionals for calculation of ground-state binding energies per nucleon and determination of potential energy surfaces (PESs) of the selected nuclei. On the other hand, pairing correlations is an important physical quantity in investigations of open shell nuclei. Generally, pairing has

been considered in the Bardeen–Cooper–Schrieffer (BCS) approach phenomenologically by regarding monopole pairing force, adjusted to the experimental mass differences of odd–even nuclei which can be a poor approximation in many cases. Because of this reason, a new formulation for pairing has been considered in the relativistic Hartree–Bogoliubov (RHB) model where the particle–particle channel of the effective inter-nucleon interaction is described by a separable finite range in pairing force (see Ref. [46] and references therein). In this study, we have considered a separable finite range pairing force and followed the prescription of Ref. [46] for triaxially symmetric RMF calculations of ^{68}Se , ^{70}Se , ^{70}Br , ^{70}Kr , ^{72}Kr , ^{74}Kr , ^{74}Rb and ^{74}Sr .

2.3. The proton-neutron Quasiparticle Random Phase Approximation (pn-QRPA) Model

The β -decay properties were studied within the quasiparticle random phase approximation with a separable multi-shell interaction on top of axially symmetric deformed mean-field calculations employing Nilsson potential. The following Hamiltonian was chosen for solution in the pn-QRPA model

$$H^{pnQRPA} = H^{sp} + V_{GT}^{ph} + V_{GT}^{pp} + V^{pair}, \quad (10)$$

where, H^{sp} corresponds to the single-particle Hamiltonian, V_{GT}^{pp} and V_{GT}^{ph} represent the particle-particle and particle-hole GT forces, respectively. The particle-particle (pp) force was initially neglected for the computation of β^- decay [47]. Later investigations revealed that this force is essential for an accurate determination of β^+ decay [48]. The pp and ph interaction strengths, characterized by κ and χ , respectively were parametrized following a $1/A^{0.7}$ dependence, as proposed in Ref. [49]. The last term in Eq. (10) denotes the pairing force and was calculated using the BCS approach. For computing the single-particle energies and wavefunctions, the Nilsson model [50] with incorporation of quadrupole deformation parameter (β_2) was employed. The oscillator constant for nucleons was determined using $\hbar\omega = (45A^{-1/3} - 25A^{-2/3})$ MeV. The same value of oscillator constant was applied for protons and neutrons. The Nilsson-potential parameters were adopted from Ref. [51]. Q -values were taken from Ref. [52]. Traditional pn-QRPA calculations used $\Delta_p = \Delta_n = 12/\sqrt{A}$ MeV [48]. However, recent findings [53] revealed that the three-term formula, based on neutron and proton separation energies, resulted in overall best prediction of β -decay half-lives using the current pn-QRPA model. Pairing gaps for proton and neutron were computed

using separation energies of proton (S_p) and neutron (S_n), respectively, as follows

$$\Delta_{pp} = \frac{2}{8}(-1)^{Z+1}[S_p(A+1, Z+1) + S_p(A-1, Z-1) - 2S_p(A, Z)] \quad (11)$$

$$\Delta_{nn} = \frac{2}{8}(-1)^{A-Z+1}[S_n(A+1, Z) + S_n(A-1, Z) - 2S_n(A, Z)]. \quad (12)$$

The reduced GT transition probabilities was calculated using

$$B_{GT}(E_j) = \frac{1}{2J_i+1} |\langle j \| M_{GT} \| i \rangle|^2, \quad (13)$$

$$M_{GT} = \sum_{k,\mu} \tau_+(k) \sigma_\mu(k),$$

where τ_+ and $\sigma_\mu(k)$ are the iso-spin raising and spherical components of the spin operator, respectively. E_j are the energy levels in daughter and $\mu = (-1, 0, 1)$ denote the third component of the angular momentum of the nucleons.

The calculation of β -decay partial half-lives was performed using

$$t_{1/2}^p = \frac{C}{(g_V/g_A)^2 f_A(A, Z, E) B_{GT}(E_j) + f_V(A, Z, E) B_F(E_j)}, \quad (14)$$

where $E = (Q - E_j)$, $g_A/g_V = -1.254$ and $C = 6295 \text{ s}$. $f_{A/V}$ are the Fermi integral functions for axial vector and vector transitions. B_{GT} (B_F) stands for the reduced transition probability for the GT (Fermi) transitions. The total β -decay half-lives were computed using

$$T_{1/2} = \left(\sum_{0 \leq E_j \leq Q} \frac{1}{t_{1/2}^p} \right)^{-1}. \quad (15)$$

For details on complete solution of Eq. (10), not reproduced here for space consideration, we refer to [48].

3. Results and Discussions

The current investigation explores the effect of quadrupole deformation parameters (β_2) on β -decay observables. To do the needful, four different deformation parameters were computed using the RMF model using the DD-ME2 and DD-PC1 functionals. Each functional yielded two local minima in the PESs, one

each for oblate (O) and prolate (P) shapes. These are referred to as $\beta_2(\text{DD-ME2 (O)})$, $\beta_2(\text{DD-ME2 (P)})$, $\beta_2(\text{DD-PC1 (O)})$ and $\beta_2(\text{DD-PC1 (P)})$, respectively. The IBM-1 model yielded spherical shapes for all selected nuclei and are denoted by $\beta_2(\text{IBM-1 (S)})$. In addition, two more β_2 were included in our investigation. The FRDM [25] computed deformation values are denoted by $\beta_2(\text{FRDM})$ and measured deformation are denoted by $\beta_2(\text{NNDC})$ taken from Ref. [26].

For the calculation of energy levels of even-even nuclei in the $A \sim 70$ region, the multipole form of IBM-1 Hamiltonian given in Eq. (1) was used. There are four free parameters ε , κ , κ' and χ in the model. Initially, Hamiltonian parameters were fitted for ^{68}Se and later expanded for heavier nuclei up to ^{74}Sr . In order to perform the fitting procedure, ε was first arranged. Later, κ , κ' and χ parameters were determined by achieving a best-fit with the experimental data [26]. The set of fitted parameters are given in Table 1. The low-lying energy spectra of selected nuclei are exhibited in Fig. 1. It may be noted from the figure that the calculated results are in good agreement with the experimental data [26]. The energy levels of unknown ^{70}Kr isotope were predicted by using the set of parameters of ^{72}Kr . Similarly, unknown energy levels in the ground state band of ^{74}Sr were predicted and shown as dotted lines in Fig. 1. The PESs as a function of deformation parameters (β , γ) for each nucleus are depicted in top panels of Fig. 1. These PESs were plotted by using the common set of fitted parameters given in Table 1. It is noted that IBM-1 predicts spherical shapes for all nuclei. Accordingly their deformation parameters are determined as *zero*.

The non-linear version of the RMF model was used to calculate various fundamental ground-state properties of nuclei including binding energy per nucleon (BE/A), nucleon separation energies, nuclear charge radii, deformations and electric moments throughout the nuclear chart [54, 55]. The RMF model, with a small number of adjustable parameters, provides the correct prediction of ground-state energies, sizes, and deformations of nuclei [37]. In the current investigation, we present the RMF model calculation, with density-dependent forces, for BE/A , two-nucleon separation energies and β_2 values of selected neutron-deficient nuclei.

In Fig. 2, the calculated BE/A values of the selected nuclei with DD-ME2 and DD-PC1 functionals are presented. Our results are compared with RMF model with NL3* interaction [54], Hartree-Fock Bogoliubov (HFB) method with SLy4 parameter set [56], Finite Range Droplet Model (FRDM) [25] and experimental data [57]. All theoretical models predict BE/A values consistent with experimental data. The best theoretical results were obtained with the FRDM data. The maximum deviation of FRDM from experimental data is 0.006 MeV while those

of other models go up to 0.06 MeV. Root mean square errors (RMSE) between model prediction values and experimental data are (0.061, 0.045, 0.062, 0.022, 0.008) MeV for RMF+DD-ME2, RMF+DD-PC1, RMF+NL3*, HFN+SLy4 and FRDM, respectively. It should be noted that HFB and RMF model results were obtained with a smaller number of adjustable parameters.

We computed two-neutron (S_{2n}) and two-proton (S_{2p}) separation energies of selected nuclei using the calculated BE values. In our calculations, we used $S_{2n} = BE(Z, N) - BE(Z, N - 2)$ and $S_{2p} = BE(Z, N) - BE(Z - 2, N)$ for determination of two-nucleon separation energies. Fig. 3 presents the calculated S_{2n} (a) and S_{2p} (b) values of ^{68}Se , ^{70}Se , ^{70}Br , ^{70}Kr , ^{72}Kr , ^{74}Kr , ^{74}Rb and ^{74}Sr together with available theoretical and experimental data. It is noted from Fig. 3(a) and 3(b), all theoretical estimates for S_{2n} and S_{2p} are in good agreement. The HFB method with SLy4 force [56] predicted values show a small deviation from the measured data.

One of the important properties of nuclei is their ground-state deformation. We employed axially deformed self-consistent RMF calculations with DD-ME2 and DD-PC1 density-dependent interactions to investigate oblate and prolate shape configurations. The PESs quantitatively determine the ground-state shape of the nuclei. The PESs of ^{68}Se , ^{70}Se , ^{70}Br , ^{70}Kr , ^{72}Kr , ^{74}Kr , ^{74}Rb and ^{74}Sr isotopes were obtained by applying the constrained triaxially symmetric RMF model calculations. The computed PESs with DD-ME2 and DD-PC1 functionals are shown in Fig. 4 and Fig. 5, respectively. In both figures, the PESs of selected nuclei are presented on a $\beta_2 - \gamma$ plane ($0 \leq \gamma \leq 60^\circ$). The binding energy was set to zero at the minimum of each surface, whereas the peripheral lines represent a step of 0.75 MeV. The PESs determined using the DD-ME2 and DD-PC1 interactions are similar to each other. In PESs of ^{70}Se , ^{70}Br , ^{70}Kr and ^{72}Kr , the minimum energy configuration was obtained on the γ -axis. This translates to oblate shape prediction for these nuclei. On the other hand, two minimum energy configurations, one on the γ -axis and the one on β_2 -axis, were obtained in the PESs of ^{68}Se , ^{74}Kr , ^{74}Rb and ^{74}Sr . In these nuclei, both DD-ME2 and DD-PC1 functional produce almost equal ground-state binding energies for oblate and prolate shapes. This means that the RMF model predicts two possible shape configurations (oblate and prolate) for ^{68}Se , ^{74}Kr , ^{74}Rb and ^{74}Sr . These deformation values were later used to investigate β -decay observables which we discuss next.

The β -decaying properties of the selected nuclei were calculated in a microscopic fashion using the pn-QRPA model. We start the proceedings by presenting a comparison of our pn-QRPA calculated GT strength distributions with the measured data in order to check reliability of the current model. For most of the nuclei

under study, experimental information on GT strength distributions are not available in the literature. Therefore, we were compelled to show the comparison for three other nuclei but having $A \sim 70$. We applied a smearing technique involving Lorentzian fitting to the theoretical strength distributions. The artificial width, applied in the fitting process, was determined based on the calculated spectrum. This widely employed technique (e.g., [58, 59, 60, 61]) entails comparing experimental data, measured in MeV^{-1} units, with theoretically derived strength distributions. Fig. 6 shows the comparison of measured and calculated GT distributions for ^{76}Sr , ^{76}Rb and ^{76}Se . The measured GT distribution for ^{76}Se was taken from Ref. [62] whereas data for ^{76}Rb and ^{76}Sr were taken from Ref. [63]. A decent comparison between calculated and measured GT strength distributions for ^{76}Sr , ^{76}Rb and ^{76}Se can be seen from Fig. 6 in $(\text{GT})_+$ directions. After validation of our nuclear model, we present our GT calculations of ^{74}Kr (Fig. 7) as a function of deformation parameter. Once again we applied the smearing technique involving Lorentzian fitting to the theoretical strength distributions. The different calculated GT distributions are compared with the measured data [64]. We denote the pn-QRPA calculated results using $\beta_2(\text{DD-ME2 (O)})$, $\beta_2(\text{DD-ME2 (P)})$, $\beta_2(\text{DD-PC1 (O)})$, $\beta_2(\text{DD-PC1 (P)})$, $\beta_2(\text{IBM-1 (S)})$ and $\beta_2(\text{FRDM})$ as $\text{QRPA}_{\beta_2(\text{DD-ME2(O)})}$, $\text{QRPA}_{\beta_2(\text{DD-ME2(P)})}$, $\text{QRPA}_{\beta_2(\text{DD-PC1(O)})}$, $\text{QRPA}_{\beta_2(\text{DD-PC1(P)})}$, $\text{QRPA}_{\beta_2(\text{IBM-1(S)})}$ and $\text{QRPA}_{\beta_2(\text{FRDM})}$, respectively. Calculated pn-QRPA strength distributions with input deformation parameters from the RMF model with DD-ME2 (O) and DD-PC1 (O) functionals (namely $\text{QRPA}_{\beta_2(\text{DD-ME2(P)})}$ and $\text{QRPA}_{\beta_2(\text{DD-PC1(O)})}$) show good comparison with the experimental data specially for the low-lying transitions between (0 - 0.5) MeV.

Figures (8 - 15) display the calculated GT strength distributions for the eight neutron-deficient nuclei. The abscissa shows the excitation energies in daughter nucleus and extends up to the Q_{β^+} value. Each figure consists of six panels and the inset shows the type of interaction used to determine the β_2 values. The strength distributions display variations as β_2 values change. The calculated distributions remain almost unchanged for the $\text{QRPA}_{\beta_2(\text{DD-PC1(O)})}$ & $\text{QRPA}_{\beta_2(\text{DD-ME2(O)})}$ and for the $\text{QRPA}_{\beta_2(\text{DD-PC1(P)})}$ & $\text{QRPA}_{\beta_2(\text{DD-ME2(P)})}$ models, as the calculated β_2 values are quite close to each other. The $\text{QRPA}_{\beta_2(\text{IBM-1(S)})}$ results predicted all nuclei to be spherical. This led to less fragmented strength distributions. Spherical deformation leads to concentration of most of the strength in few states [48].

Tables (2 - 9) present the calculated state-by-state GT strength distributions, branching ratios, and partial half-lives as a function of β_2 values for ^{68}Se , ^{70}Se , ^{70}Br , ^{70}Kr , ^{72}Kr , ^{74}Kr , ^{74}Rb & ^{74}Sr , respectively. The branching ratio (I) was

computed using

$$I = \frac{T_{1/2}}{t_{1/2}^p} \times 100 (\%). \quad (16)$$

Transitions possessing branching ratios greater than 1% only are shown in Tables (2 - 9). It is again noted that the spherical deformation values led to smaller fragmentation of the GT strength in daughter states.

Tables (10 - 11) show the calculated deformation parameters, total GT strength & centroid values, measured and calculated half-lives for selected nuclei. The last column in the tables is a measure of the predictive power of the pn-QRPA model using different β_2 values. The ratio R_i was defined using

$$R_i = \begin{cases} T_{1/2}^{cal}/T_{1/2}^{exp} & \text{if } T_{1/2}^{cal} \geq T_{1/2}^{exp} \\ T_{1/2}^{exp}/T_{1/2}^{cal} & \text{if } T_{1/2}^{exp} > T_{1/2}^{cal}. \end{cases} \quad (17)$$

The nuclei selected for the current investigation find their respective positions far away from the β -stability line. It is noted from Tables (10 - 11) that the FRDM and RMF models predicted large deformations for these nuclei. The measured β_2 values were available only for four cases and suggested deformed shapes for these nuclei. Bigger total GT strength and smaller values of the centroid result in shorter computed β -decay half-lives. For the case of ^{70}Br and ^{74}Rb , both the RMF and FRDM predicted β_2 values resulted in larger deviations in the calculated half-lives. Measured deformation values were not present for both these nuclei. For the case ^{74}Rb , there is large deviation between the half-lives computed using $\text{QRPA}_{\beta_2(DD-PC1(O))}$ & $\text{QRPA}_{\beta_2(DD-ME2(O))}$ interactions, even though the deformations are almost comparable. The reason is that the $\text{QRPA}_{\beta_2(DD-ME2(O))}$ leads to higher computed cumulative strength and lower centroid value as compared to $\text{QRPA}_{\beta_2(DD-PC1(O))}$ interaction, which led to smaller computed half life value. Tables (10 - 11) show that the computed R_i value for most of the cases is within 2, implying the model reproduces most of the experimentally known half-lives within a factor of 2. Small R_i values demonstrate the effectiveness of the pn-QRPA model. It was commented that the pn-QRPA model gives better prediction for nuclei far off from the line of stability [48, 47].

Table 12 shows overall standings of the accuracy of the pn-QRPA model as a function of the computed β_2 values. The average ratio (\bar{R}) was defined as

$$\bar{R} = \frac{\sum_{i=1}^n R_i}{n}, \quad (18)$$

where n is the number of nuclei. The lowest ratio was reported for $\text{QRPA}_{\beta_2(NNDC)}$. However, it is remarked that this average was computed only for four out of the eight selected cases and may not be treated as a reliable data. Amongst the other models, the $\text{QRPA}_{\beta_2(DD-ME2(O))}$ resulted in the smallest \bar{R} value. This is closely followed by the $\text{QRPA}_{\beta_2(FRDM)}$ results. The $\text{QRPA}_{\beta_2(DD-PC1(P))}$ and $\text{QRPA}_{\beta_2(IBM-1(S))}$ predicted rather poor half-lives.

4. Summary and Conclusion

In this paper, we report the ground-state deformations and investigations on possible shape co-existence for $A \sim 70$ nuclei.

We calculated energy levels of even-even nuclei by fitting parameters of the IBM-1 Hamiltonian and obtained results in close proximity with the experimental data. Using the same set of parameters the PESs were plotted that predicted spherical shapes for the selected nuclei.

The RMF model with density-dependent meson exchange (DD-ME2) and point coupling (DD-PC1) interactions was later employed to compute binding and two-nucleon separation energies for the eight selected neutron-deficient nuclei. The calculated quantities were in agreement with the measured data. The calculated PESs were used for determination of ground-state shape of the selected nuclei. Both (DD-ME2 and DD-PC1) functionals produced similar PESs and predicted oblate configurations for ^{70}Se , ^{70}Br , ^{70}Kr and ^{72}Kr nuclei. A possible shape co-existence (oblate and prolate) was supported by the RMF model for ^{68}Se , ^{74}Kr , ^{74}Rb and ^{74}Sr nucleus. On the other hand, the IBM-1 predicted *zero* values for deformation parameters.

The pn-QRPA model with a schematic and separable potential was later employed to calculate β -decay properties of $A \sim 70$ nuclei. The different set of β_2 values including ones obtained from IBM-1 and RMF models were used as inputs to perform the systematic pn-QRPA calculations for the given neutron-deficient nucleus. The model has an excellent track-record for predicting half-lives of nuclei far-off from line of stability. Our investigation supported shape co-existence phenomena for neutron-deficient $A \sim 70$ nuclei. The predicted half-lives using $\text{QRPA}_{\beta_2(DD-ME2(P))}$ & $\text{QRPA}_{\beta_2(DD-ME2(O))}$ were in best agreement with the measured data. Our findings may prove useful for further investigation of the rp -process waiting points.

Acknowledgments

J.-U. Nabi would like to acknowledge the support of the Higher Education Commission Pakistan through project number 20-15394/NRPU/R&D/HEC/2021.

References

- [1] A. N. Bohr and B. R. Mottelson, *Kgl. Danske Videnskab. Selskab, Dan. Mat-fys. Medd* **27**, No. 16 (1953).
- [2] H. Morinaga, *Phys. Rev.* **1(101)**, 254 (1956).
- [3] K. Heyde and J. L. Wood, *Rev. Mod. Phys.* **83**, 1467 (2011).
- [4] P. E. Garrett, M. Zielinska, E. Clement, *Prog. Part. Nucl. Phys.* **124**, 103931 (2022).
- [5] O. Moreno, P. Sarriguren, R. Alvarez-Rodriguez, E. M. De Guerra, *Phys. Rev. C* **73(5)**, 054302 (2006).
- [6] N. Bree, K. Wrzosek-Lipska, A. Petts, A. Andreyev, B. Bastin, M. Bender, A. Blazhev, B. Bruyneel, P. A. Butler, J. Butterworth, M. P. Carpenter, *Phys. Rev. Lett.* **16(112)**, 162701 (2014).
- [7] W. McLatchie, J. E. Kitching, W. Darcey, *Phys. Lett. B* **30**, 529 (1969).
- [8] F. Frisk, I. Hamamoto, X. Z. Zhang, *Phys. Rev. C* **52**, 2468 (1995).
- [9] P. Sarriguren, E. Moya de Guerra, A. Escuderos, A. C. Carrizo, *Nucl. Phys. A* **635**, 55 (1998).
- [10] P. Sarriguren, *Phys. Rev. C* **79**, 044315 (2009); *Phys. Lett. B* **680**, 438 (2009); *Phys. Rev. C* **83**, 025801 (2011).
- [11] P. Sarriguren, *Phys. Rev. C* **87**, 045801 (2013).
- [12] P. Sarriguren, J. Pereira, *Phys. Rev. C* **81**, 064314 (2010); P. Sarriguren, A. Algora, J. Pereira, *Phys. Rev. C* **89**, 034311 (2014).
- [13] E. Poirier et al., *Phys. Rev. C* **69**, 034307 (2004); E. Nacher et al., *Phys. Rev. Lett.* **92**, 232501 (2004); A. B. Perez-Cerdan et al., *Phys. Rev. C* **88**, 014324 (2013).

- [14] A. Petrovici, et al., *Phys. Rev. C*, **78** 044315 (2008).
- [15] J. -U. Nabi, M. Büyükata, *Nucl. Phys. A*, **947** 182 (2016).
- [16] J. -U. Nabi, M. Büyükata, *Astrophys Space Sci.* **362** 9 (2017).
- [17] J. -U. Nabi, M. Ishfaq, M. Büyükata, M. Riaz, *Nucl. Phys. A*, **966** 1 (2017).
- [18] P. J. Davies, et al., *Phys. Rev. C* **99**, 021302(R) (2021).
- [19] W. Nazarewicz, J. Dudek, R. Bengtsson, I. Ragnarsson, *Nucl. Phys. A* **435** 397 (1985).
- [20] P. Bonche, H. Flocard, P. H. Heenen, S. J. Kreiger, M. S. Weiss, *Nucl. Phys. A* **443** 39 (1985).
- [21] A. Petrovici, K. W. Schmid, A. Faessler, *Nucl. Phys. A* **647** 197 (1999).
- [22] A. Petrovici *Phys. Rev. C*, **91** 014302 (2015).
- [23] A. Petrovici, et al., *Nucl. Phys. A*, **665** 333-350 (2000).
- [24] H. Schatz, et al., *Phys. Rep.*, **294** 167 (1998).
- [25] P. Moller, et al., *At. Data Nucl. Data Tables* **109110**, 1 (2016).
- [26] National Nuclear Data Center (NNDC), <http://www.nndc.bnl.gov/> (2023).
- [27] F. Iachello, A. Arima, *Interacting Boson Model*, Cambridge University Press (1987).
- [28] R. F. Casten, D. D. Warner, *Rev. Mod. Phys.* **60** 389 (1988).
- [29] A. E. L. Dieperink, O. Scholten 1980 *Nucl. Phys. A* **346** 125.
- [30] J. N. Ginocchio, M. W. Kirson 1980 *Nucl. Phys. A* **350** 31.
- [31] A. N. Bohr and B. R. Mottelson, *Nuclear Structure* (in 2 volumes), World Scientific Publishing Company (1998)
- [32] B. D. Serot, J. D. Walecka, *Adv. Nucl. Phys.* **16**, 1 (1986).
- [33] B. D. Serot, J. D. Walecka, *Internat. J. Modern Phys. E* **6**, 515 (1997).

- [34] J. Boguta and A. R. Bodmer, *Nucl. Phys. A* **292**, 413 (1977).
- [35] T. Nikšić and D. Vretenar and P. Ring, *Prog. Part. Nucl. Phys.* **66**, 519 (2011).
- [36] G. A. Lalazissis, J. König and P. Ring, *Phys. Rev. C* **55**, 540 (1997).
- [37] P. Ring, *Prog. Part. Nucl. Phys.* **37**, 193 (1996).
- [38] S. Typel and H. H. Wolter, *Nucl. Phys. A* **656**, 331 (1999).
- [39] D. Vretenar, A. V. Afanasjev and G. A. Lalazissis, *Phys. Rep.* **409**, 101 (2005).
- [40] J. Meng, H. Toki, S. G. Zhou, S. Q. Zhang, W. H. Long, and L. S. Geng, *Prog. Part. Nucl. Phys.* **57**, 470 (2006).
- [41] S. Haddad, *Acta Phys. Pol. B* **38**, 2121 (2007).
- [42] X. Roca-Maza, X. Vinas, M. Centelles, P. Ring and P. Schuck, *Phys. Rev. C* **84**, 054309 (2011).
- [43] S. Typel, *Particles* **1** 3 (2018).
- [44] G. A. Lalazissis, T. Nikšić, D. Vretenar and P. Ring, *Phys. Rev. C* **71**, 024312 (2005).
- [45] T. Nikšić, D. Vretenar and P. Ring, *Phys. Rev. C* **78**, 034318 (2008).
- [46] T. Nikšić, N. Paar, D. Vretenar and P. Ring, *Computer Physics Communications*, **185**, 1808 (2014).
- [47] A. Staudt, E. Bender, K. Muto, H. V. Klapdor-Kleingrothaus, *At. Data Nucl. Data Tables* **44** 79-132 (1990).
- [48] M. Hirsch, A. Staudt, K. Muto, H. V. Klapdor-Kleingrothaus, *At. Data Nucl. Data Tables* **53** 165-193 (1993).
- [49] H. Homma, E. Bender, M. Hirsch, K. Muto, H. Klapdor-Kleingrothaus, T. Oda, *Phys. Rev. C* **54**, 2972 (1996).
- [50] S. G. Nilsson, *Mat. Fys. Medd. Dan. Vid. Selsk* **29**, 16 (1955).

- [51] I. Ragnarsson, R. K. Sheline, *Phys. Scripta* **29**, 385 (1984).
- [52] F. G. Kondev, M. Wang, W. J. Huang, S. Naimi, G. Audi, *Chin. Phys. C* **45**, 030001 (2021).
- [53] A. Ullah, J.-U. Nabi and M. Tahir *Braz. J. Phys.* **53:39** (2023).
- [54] T. Bayram and A. H. Yılmaz, *Mod. Phys. Lett. A* **28**, 1350068 (2013).
- [55] G. A. Lalazissis, S. Raman and P. Ring, *Atom. Data N. Data Tab.* **71**, 1 (1999).
- [56] M. V. Stoitsov, J. Dobaczewski, N. Nazarewicz, S. Pittel and D. J. Dean, *Phys. Rev. C* **68**, 054312 (2003).
- [57] M. Wang, G. Audi, F. G. Kondev, W.J. Huang, S. Naimi and X. Xu, *Chin. Phys. C* **41**, 030003 (2017).
- [58] J. Yasuda et al., *Phys. Rev. Lett.*, **121**, 132501 (2018).
- [59] C. J. Guess et al., *Phys. Rev. C*, **83**, 064318 (2011).
- [60] T. Wakasa et al., *Phys. Rev. C*, **85**, 064606 (2012).
- [61] B. Gao et al., *Phys. Rev. C*, **101**, 014308 (2020).
- [62] R. L. Helmer et al., *Phys. Rev. C*, **55**, 2802-2810 (1997).
- [63] A. B. Pérez-Cerdán et al., *Phys. Rev. C*, **88**, 014324 (2013).
- [64] E. Poirier et al., *Phys. Rev. C*, **69**, 034307 (2004).

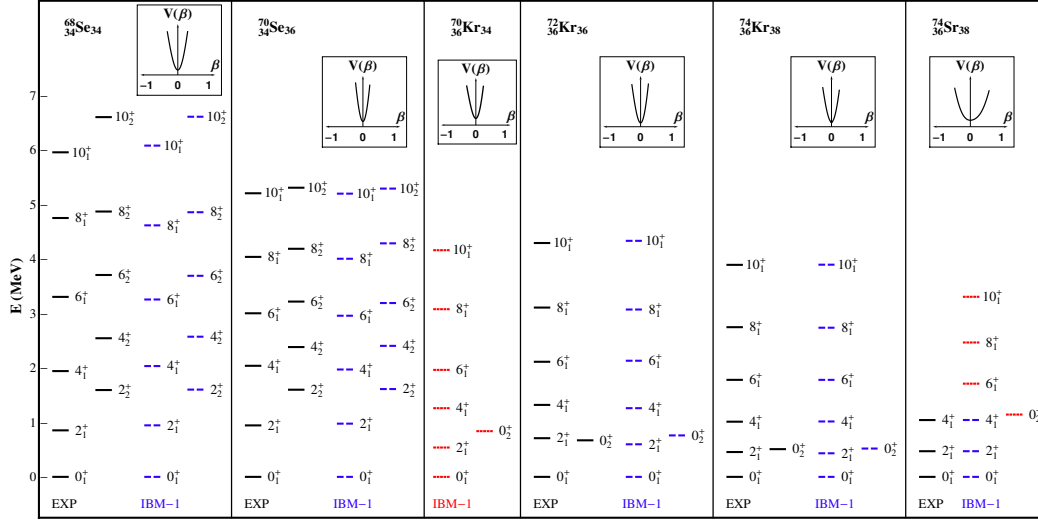


Figure 1: The experimental (solid), calculated (dashed) and predicted (dotted) energy spectra of ^{68}Se , ^{70}Se , ^{70}Kr , ^{72}Kr , ^{74}Kr , ^{74}Sr . The inset shows PESs as a function of β for $\gamma = 0^\circ$.

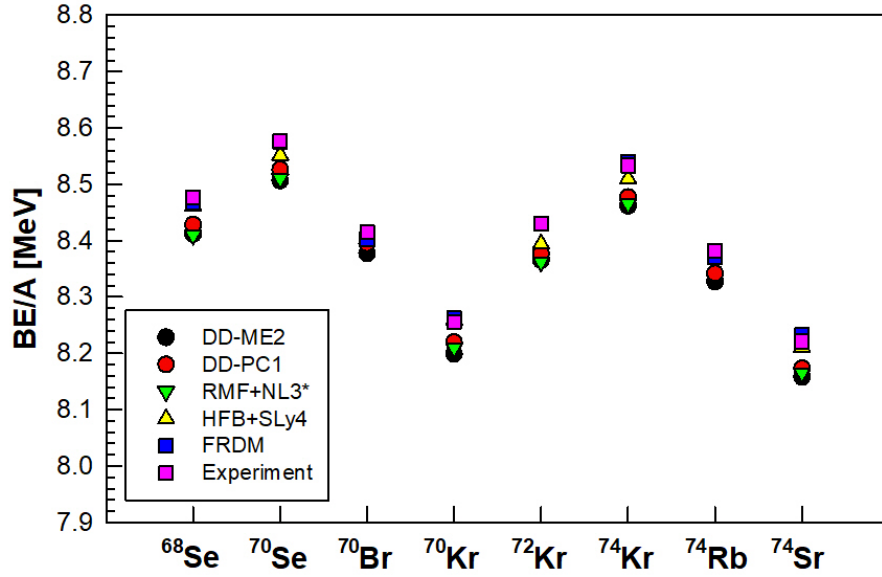


Figure 2: The calculated BE/A values with DD-ME2 and DD-PC1 functionals in comparison with the results of RMF model with NL3* interaction [54], HFB method with SLy4 force [56], FRDM [25] and experimental data [57].

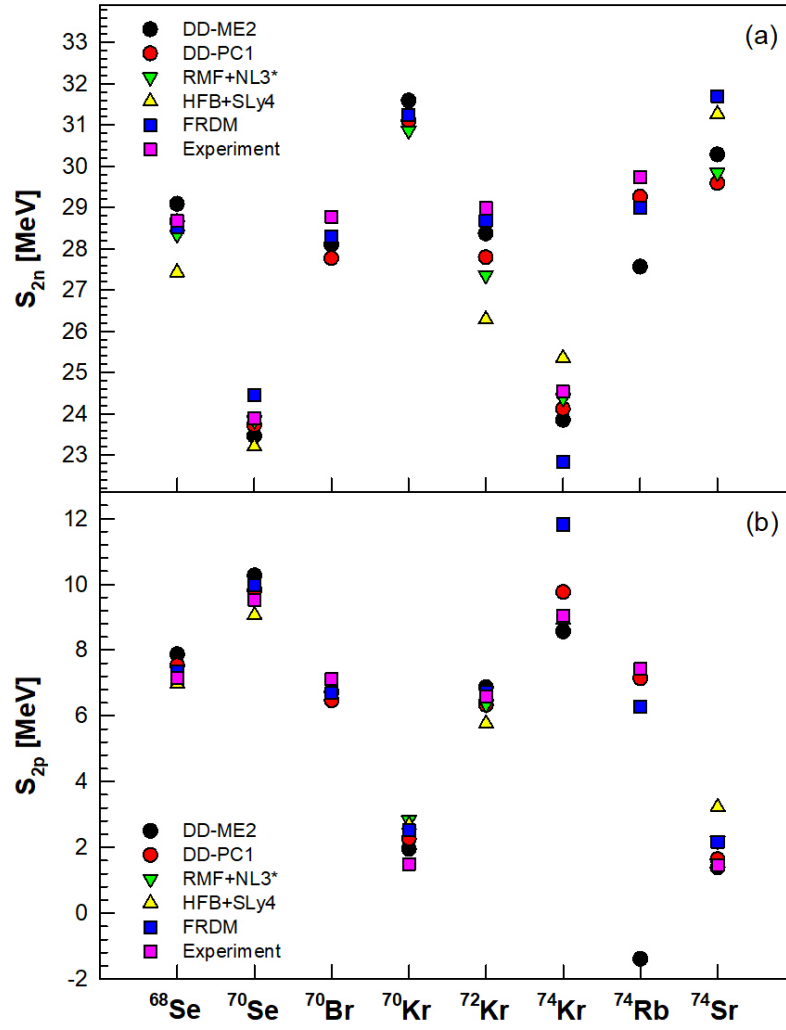


Figure 3: The calculated two-neutron (a) and two-proton (b) separation energies of selected nuclei. Shown also are the results of RMF model with NL3* interaction [54], HFB method with SLy4 force [56], FRDM [25] and experimental data [57], wherever applicable.

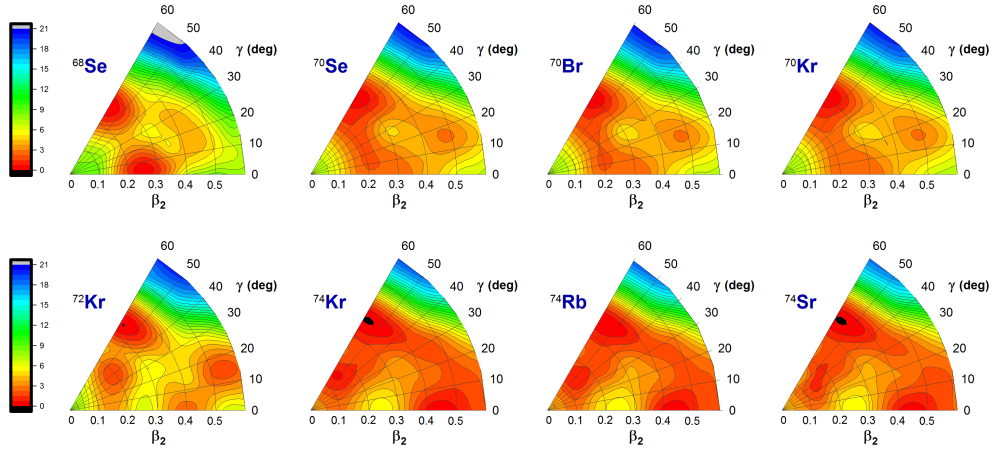


Figure 4: The PESs of ^{68}Se , ^{70}Se , ^{70}Br , ^{70}Kr , ^{72}Kr , ^{74}Kr , ^{74}Rb and ^{74}Sr obtained from DD-ME2 calculation. See text for further details.

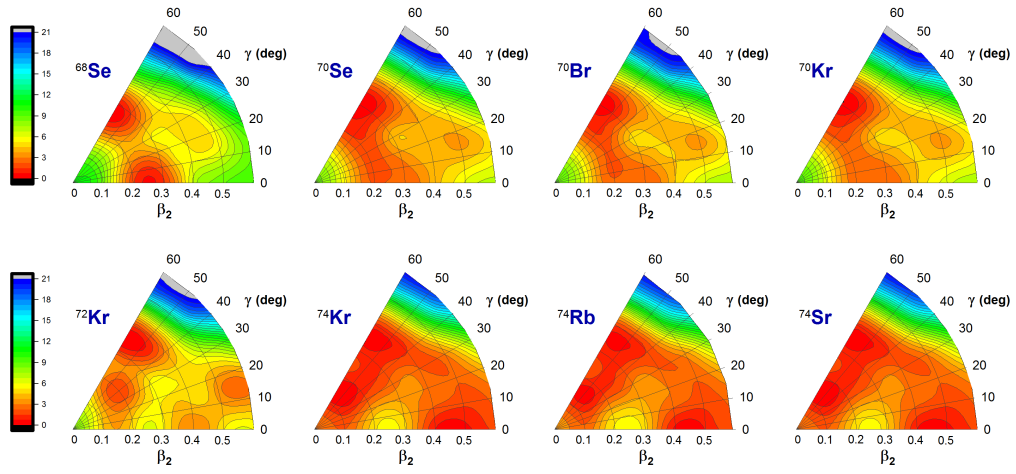


Figure 5: Same as Fig. 4 but for DD-PC1 interaction.

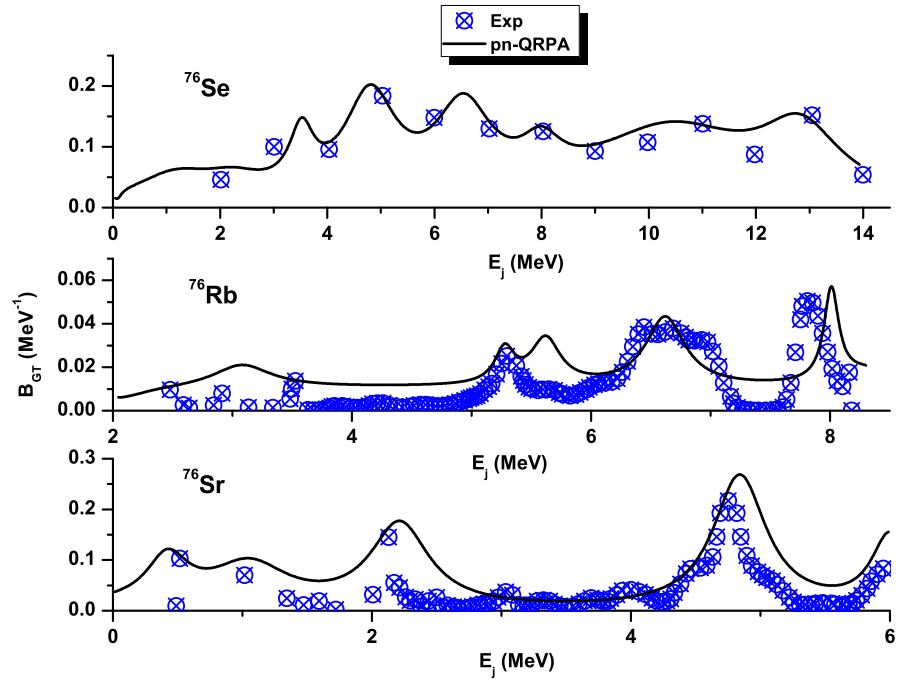


Figure 6: Comparison of pn-QRPA calculated GT_+ strength distributions of ^{76}Se , ^{76}Rb and ^{76}Sr with measured data [62, 63]. The abscissa shows excitation energies in daughter nuclei.

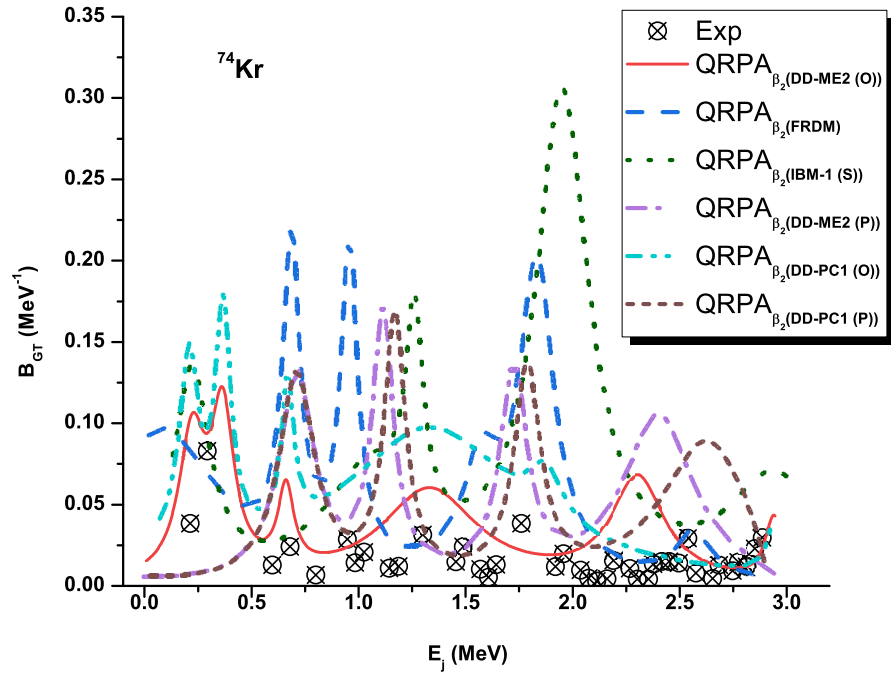


Figure 7: Comparison of pn-QRPA calculated GT_+ strength distributions of ^{74}Kr with measured data [64]. The abscissa shows excitation energies in daughter nuclei. See text for explanation of symbols.

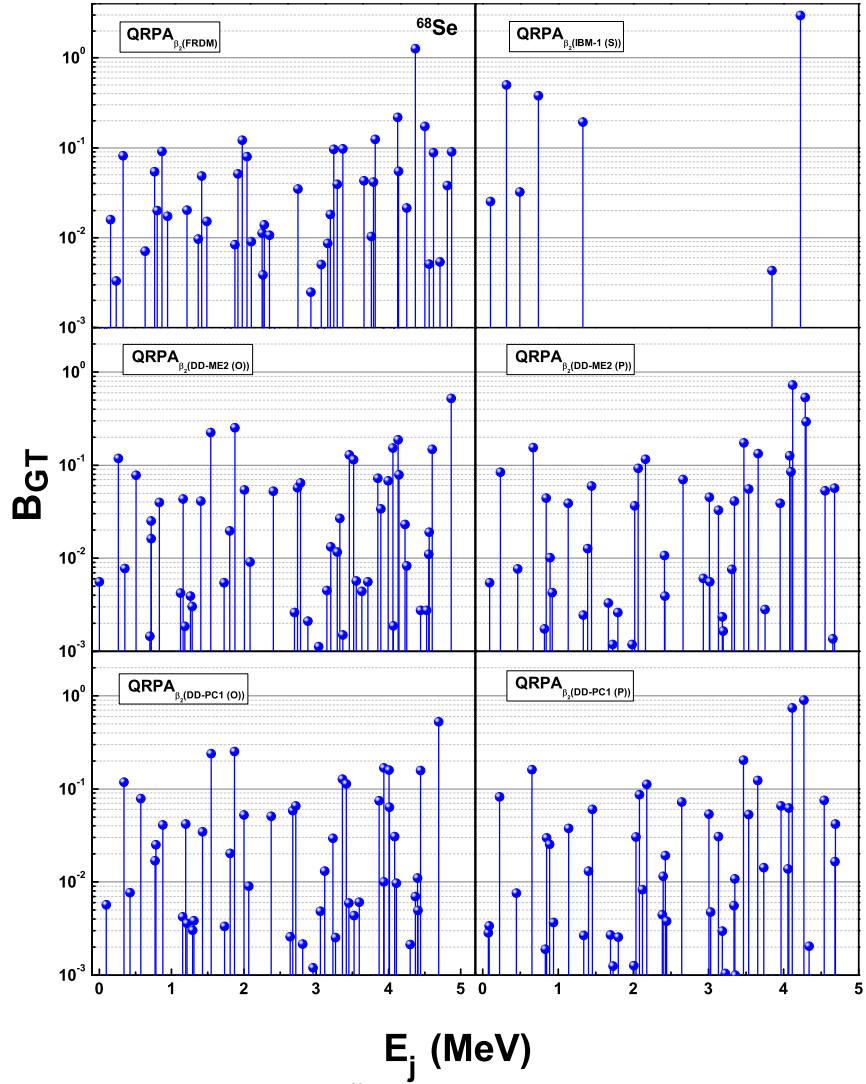


Figure 8: GT strength distributions of ^{68}Se as a function of deformation parameter obtained from models shown in the inset. The abscissa shows excitation energies in daughter nuclei.

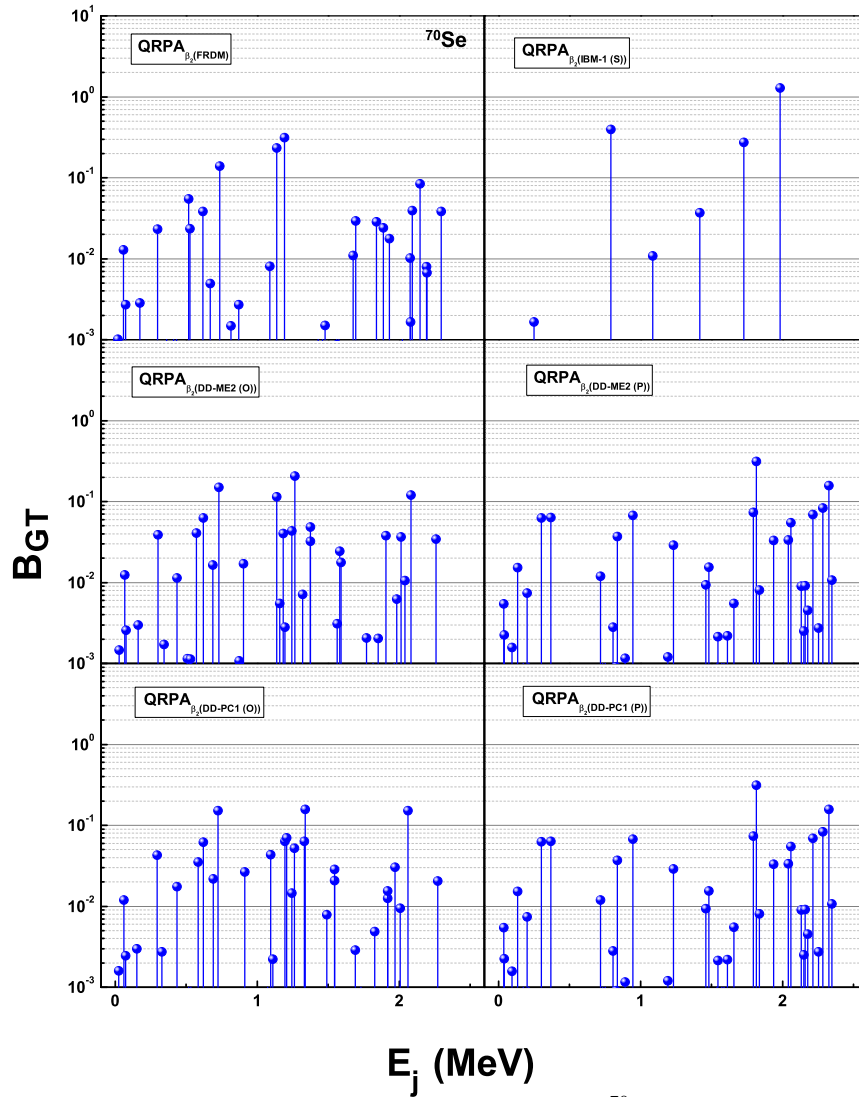


Figure 9: Same as Fig. 8 but for ^{70}Se .

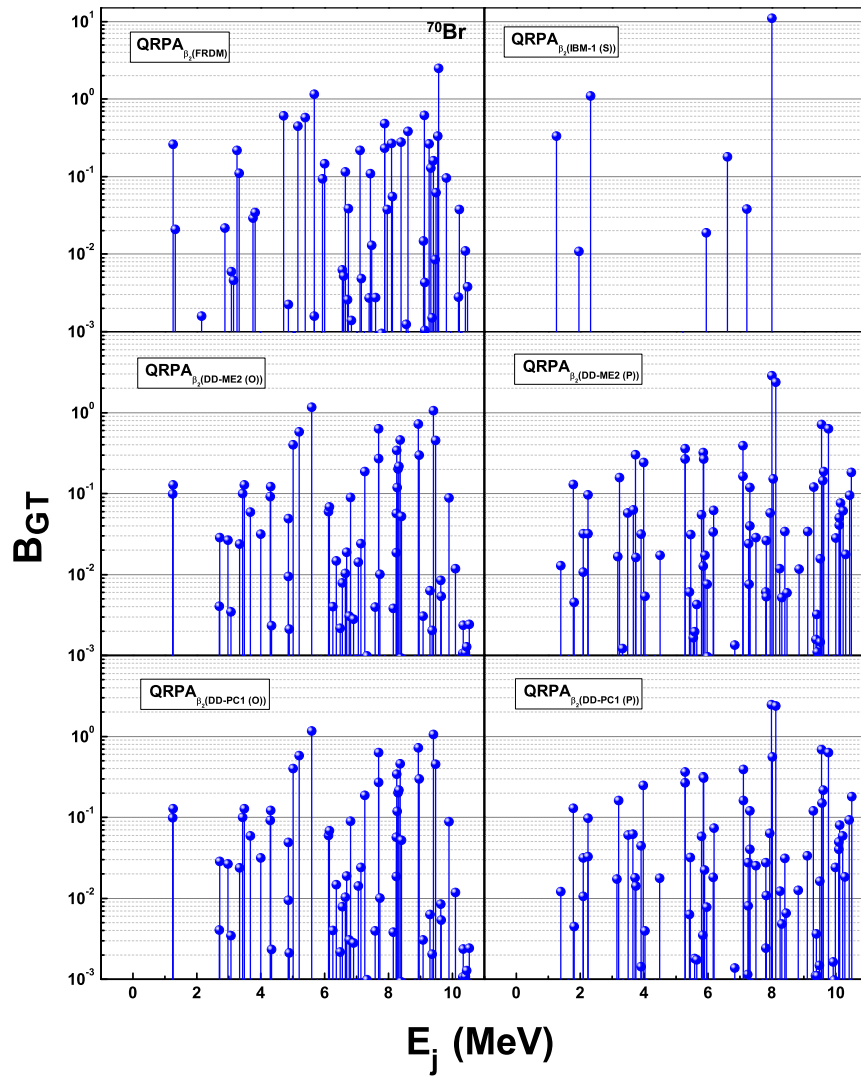


Figure 10: Same as Fig. 8 but for ^{70}Br .

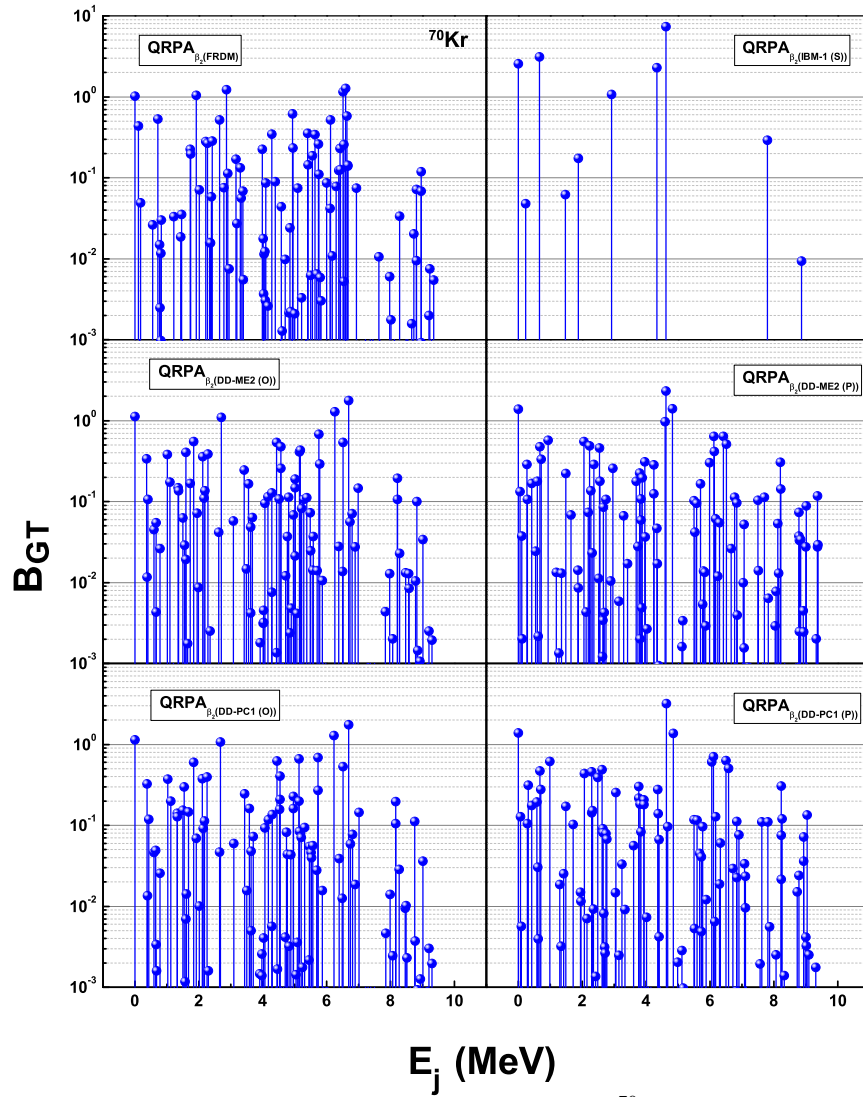


Figure 11: Same as Fig. 8 but for ^{70}Kr .

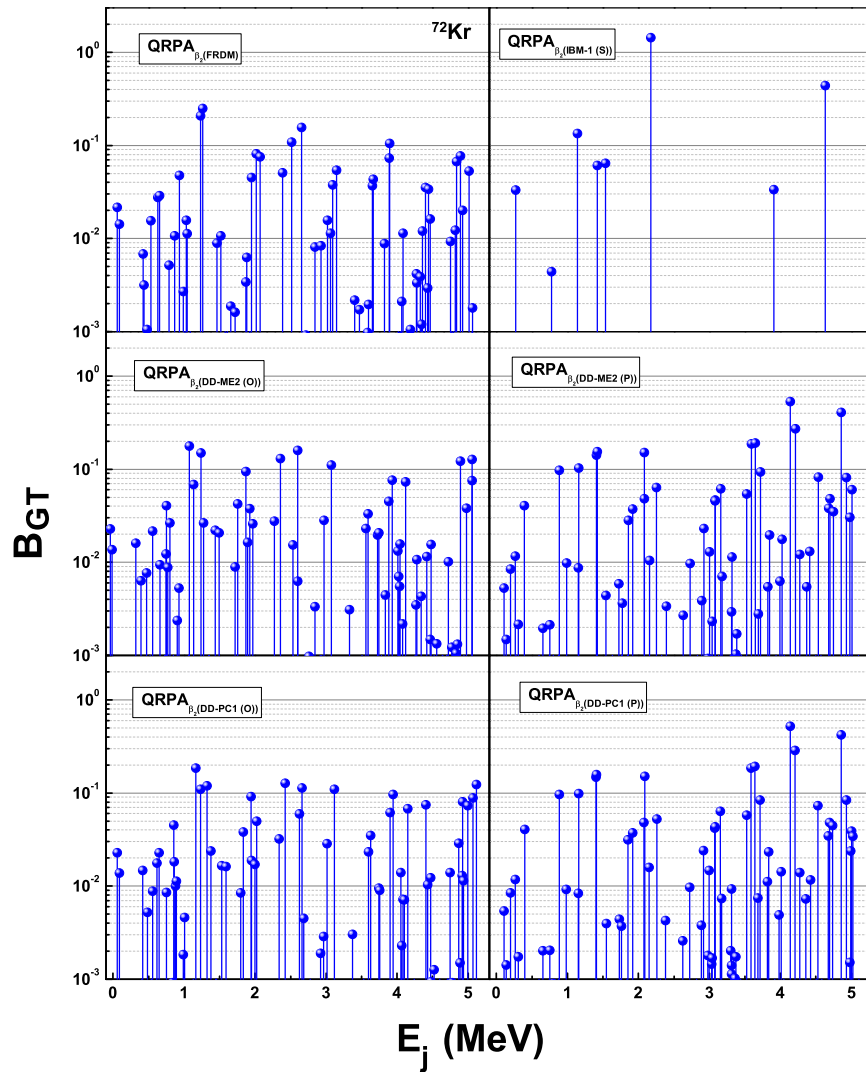


Figure 12: Same as Fig. 8 but for ^{72}Kr .

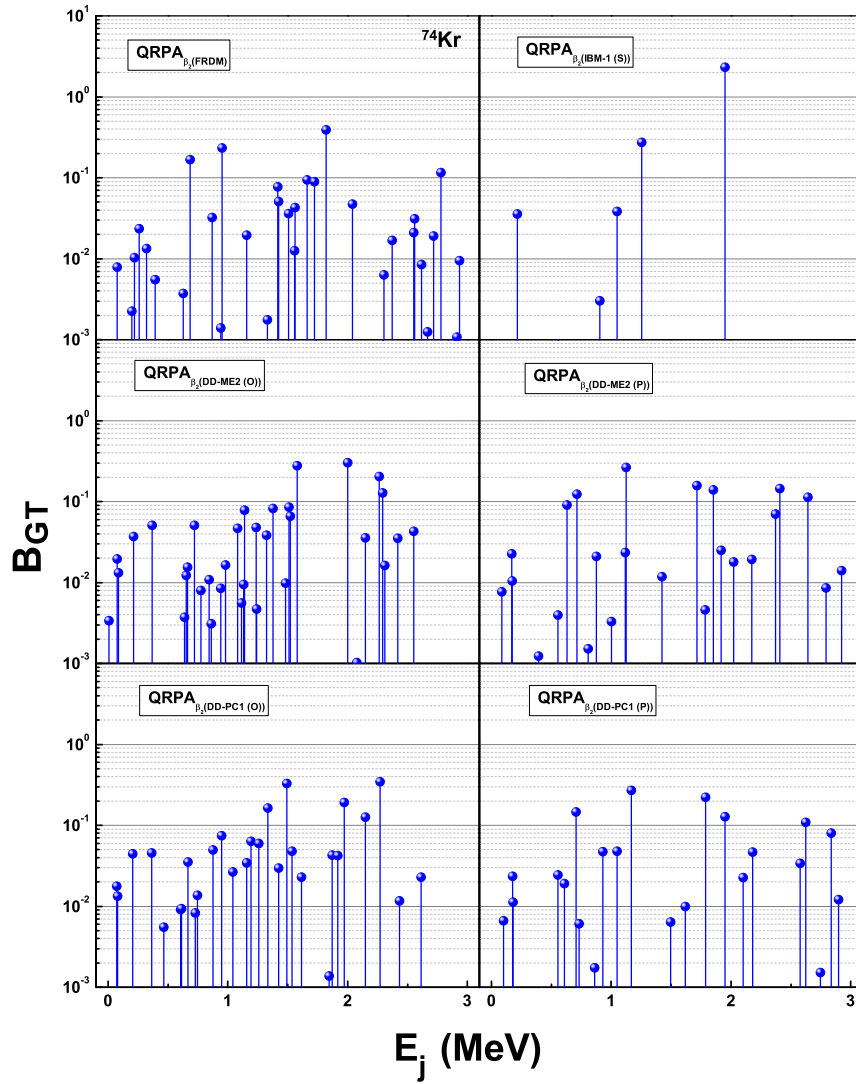


Figure 13: Same as Fig. 8 but for ^{74}Kr .

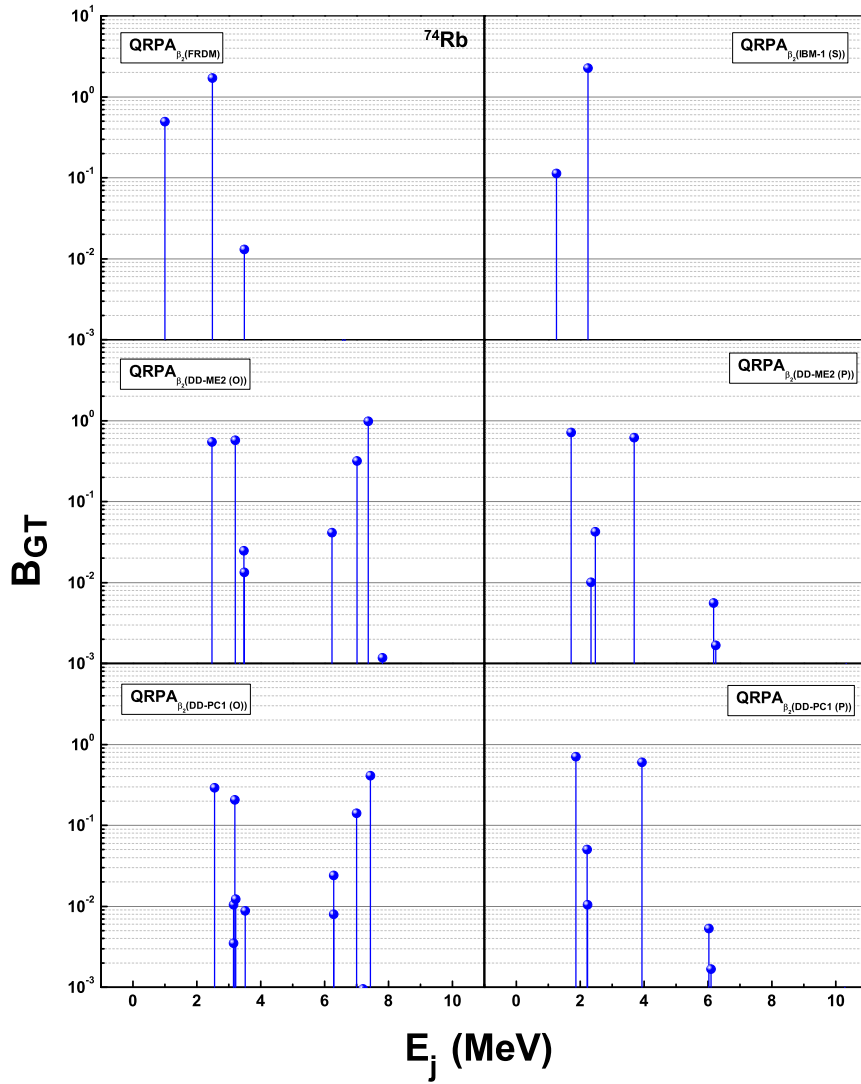


Figure 14: Same as Fig. 8 but for ^{74}Rb .

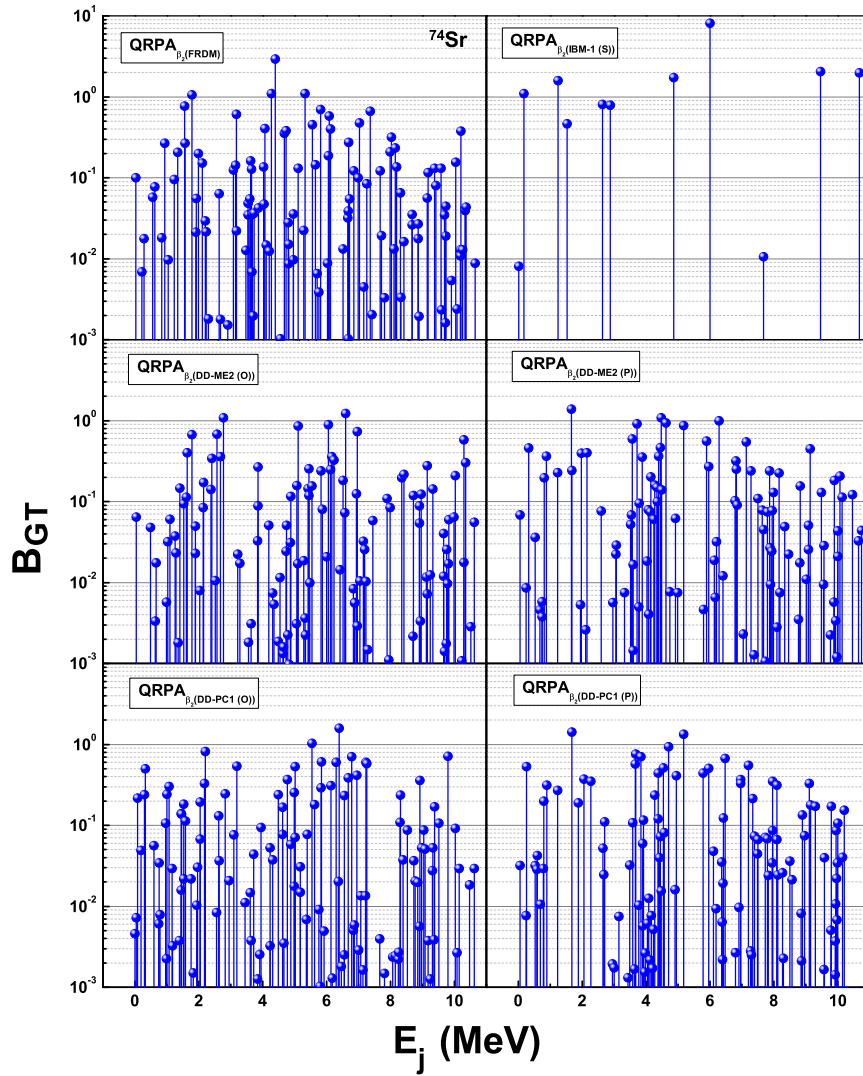


Figure 15: Same as Fig. 8 but for ^{74}Sr .

Table 1: Set of parameters of the IBM-1 Hamiltonian in units of keV. N is the number of the bosons. χ is dimensionless.

Nuclei	N	ε	κ	κ'	χ
^{68}Se	6	544.2	39.9	32.5	-0.58
^{70}Se	7	470.2	79.4	27.0	-0.29
^{70}Kr	7	203.4	46.9	29.4	-0.90
^{72}Kr	8	203.4	46.9	29.4	-0.90
^{74}Kr	8	116.0	31.0	29.4	-0.50
^{74}Sr	9	728.9	-20.5	-	-0.50

Table 2: State-by-state B_{GT} strength, branching ratios and partial half-lives calculated using the deformed pn-QRPA with six different deformation parameter values for ^{68}Se .

QRPA $_{\beta_2(FRDM)}$				QRPA $_{\beta_2(IBM-1(S))}$				QRPA $_{\beta_2(DD-ME2(O))}$			
E_j	B_{GT}	I	$t_{1/2}^p$	E_j	B_{GT}	I	$t_{1/2}^p$	E_j	B_{GT}	I	$t_{1/2}^p$
0.147	0.016	8.05	4.73E+02	0.103	0.025	4.09	2.81E+02	0.097	0.006	2.45	1.26E+03
0.222	0.003	1.52	2.51E+03	0.312	0.502	62.00	1.85E+01	0.347	0.118	37.27	8.26E+01
0.316	0.081	33.21	1.15E+02	0.489	0.032	3.14	3.66E+02	0.430	0.008	2.20	1.40E+03
0.608	0.007	1.94	1.97E+03	0.740	0.378	25.63	4.48E+01	0.575	0.078	18.06	1.70E+02
0.734	0.054	12.27	3.11E+02	1.328	0.194	5.03	2.28E+02	0.770	0.016	2.81	1.10E+03
0.766	0.020	4.33	8.81E+02					0.775	0.025	4.30	7.15E+02
0.828	0.091	17.90	2.13E+02					0.880	0.040	5.83	5.28E+02
0.904	0.017	3.03	1.26E+03					1.189	0.043	3.85	8.00E+02
1.161	0.020	2.33	1.63E+03					1.420	0.041	2.42	1.27E+03
1.360	0.049	3.94	9.67E+02					1.548	0.225	10.37	2.97E+02
1.426	0.015	1.09	3.51E+03					1.867	0.251	5.99	5.14E+02
1.843	0.051	1.60	2.39E+03								
1.901	0.122	3.34	1.14E+03								
1.961	0.080	1.92	1.98E+03								

QRPA $_{\beta_2(DD-ME2(P))}$				QRPA $_{\beta_2(DD-PC1(O))}$				QRPA $_{\beta_2(DD-PC1(P))}$			
E_j	B_{GT}	I	$t_{1/2}^p$	E_j	B_{GT}	I	$t_{1/2}^p$	E_j	B_{GT}	I	$t_{1/2}^p$
0.089	0.005	2.71	1.28E+03	0.096	0.006	2.47	1.24E+03	0.070	0.003	1.43	2.40E+03
0.231	0.084	34.83	9.92E+01	0.343	0.118	37.48	8.18E+01	0.082	0.003	1.66	2.06E+03
0.460	0.008	2.34	1.48E+03	0.428	0.008	2.18	1.41E+03	0.224	0.082	33.76	1.01E+02
0.667	0.155	35.13	9.83E+01	0.572	0.078	18.11	1.69E+02	0.445	0.008	2.33	1.46E+03
0.840	0.044	7.77	4.45E+02	0.771	0.017	2.92	1.05E+03	0.652	0.161	36.90	9.25E+01
0.893	0.010	1.64	2.11E+03	0.783	0.025	4.25	7.22E+02	0.845	0.030	5.14	6.64E+02
1.132	0.039	4.27	8.09E+02	0.877	0.041	6.00	5.11E+02	0.889	0.025	4.09	8.36E+02
1.447	0.060	3.75	9.21E+02	1.194	0.042	3.68	8.33E+02	1.138	0.038	4.05	8.42E+02
2.064	0.092	1.59	2.17E+03	1.425	0.035	2.01	1.52E+03	1.455	0.060	3.67	9.31E+02
2.164	0.115	1.57	2.21E+03	1.549	0.238	10.87	2.82E+02	2.081	0.086	1.42	2.41E+03
				1.872	0.251	5.92	5.18E+02	2.179	0.112	1.45	2.35E+03

Table 3: Same as Table 2 but for ^{70}Se .

QRPA $_{\beta_2}(\text{FRDM})$				QRPA $_{\beta_2}(\text{IBM-1}(S))$				QRPA $_{\beta_2}(\text{DD-ME2}(O))$			
E_j	B_{GT}	I	$t_{1/2}^p$	E_j	B_{GT}	I	$t_{1/2}^p$	E_j	B_{GT}	I	$t_{1/2}^p$
0.059	0.013	8.89	3.18E+04	0.250	0.002	1.11	4.06E+05	0.028	0.001	1.06	2.60E+05
0.072	0.003	1.80	1.57E+05	0.790	0.393	73.86	6.12E+03	0.066	0.012	8.18	3.36E+04
0.173	0.003	1.46	1.94E+05	1.086	0.011	1.19	3.80E+05	0.077	0.003	1.65	1.67E+05
0.297	0.023	8.71	3.25E+04	1.417	0.037	2.25	2.01E+05	0.162	0.003	1.54	1.78E+05
0.517	0.055	11.86	2.39E+04	1.728	0.274	7.76	5.83E+04	0.301	0.039	14.06	1.96E+04
0.527	0.023	4.94	5.73E+04	1.982	1.279	13.83	3.27E+04	0.434	0.011	2.93	9.40E+04
0.619	0.038	6.48	4.36E+04					0.572	0.041	7.55	3.65E+04
0.735	0.139	18.30	1.55E+04					0.622	0.062	10.24	2.69E+04
1.137	0.234	14.84	1.91E+04					0.688	0.016	2.34	1.18E+05
1.192	0.312	18.04	1.57E+04					0.730	0.151	19.52	1.41E+04
								0.903	0.017	1.58	1.74E+05
								1.139	0.115	7.09	3.89E+04
								1.182	0.040	2.30	1.20E+05
								1.244	0.044	2.24	1.23E+05
								1.266	0.206	10.21	2.70E+04
								1.374	0.032	1.30	2.12E+05
								1.376	0.048	1.95	1.41E+05

QRPA $_{\beta_2}(\text{DD-ME2}(P))$				QRPA $_{\beta_2}(\text{DD-PC1}(O))$				QRPA $_{\beta_2}(\text{DD-PC1}(P))$			
E_j	B_{GT}	I	$t_{1/2}^p$	E_j	B_{GT}	I	$t_{1/2}^p$	E_j	B_{GT}	I	$t_{1/2}^p$
0.037	0.005	4.75	7.16E+04	0.026	0.002	1.14	2.36E+05	0.037	0.005	4.75	7.16E+04
0.039	0.002	1.96	1.74E+05	0.062	0.012	7.79	3.47E+04	0.039	0.002	1.96	1.74E+05
0.095	0.002	1.19	2.85E+05	0.072	0.002	1.56	1.73E+05	0.095	0.002	1.19	2.85E+05
0.135	0.015	10.42	3.27E+04	0.152	0.003	1.54	1.75E+05	0.135	0.015	10.42	3.27E+04
0.201	0.007	4.26	7.98E+04	0.294	0.043	15.49	1.74E+04	0.201	0.007	4.26	7.98E+04
0.302	0.063	28.06	1.21E+04	0.434	0.018	4.45	6.07E+04	0.302	0.063	28.06	1.21E+04
0.369	0.063	23.83	1.43E+04	0.583	0.035	6.20	4.36E+04	0.369	0.063	23.83	1.43E+04
0.719	0.012	1.96	1.74E+05	0.622	0.062	9.99	2.70E+04	0.719	0.012	1.96	1.74E+05
0.837	0.037	4.79	7.10E+04	0.690	0.022	3.01	8.97E+04	0.837	0.037	4.79	7.10E+04
0.945	0.068	7.15	4.76E+04	0.724	0.152	19.54	1.38E+04	0.945	0.068	7.15	4.76E+04
1.232	0.029	1.87	1.82E+05	0.913	0.027	2.35	1.15E+05	1.232	0.029	1.87	1.82E+05
1.795	0.074	1.27	2.69E+05	1.096	0.043	2.82	9.59E+04	1.795	0.074	1.27	2.69E+05
1.815	0.313	5.05	6.74E+04	1.194	0.064	3.49	7.73E+04	1.815	0.313	5.05	6.74E+04
				1.208	0.070	3.74	7.22E+04				
				1.262	0.052	2.56	1.06E+05				
				1.332	0.064	2.75	9.84E+04				
				1.337	0.158	6.74	4.01E+04				

Table 4: Same as Table 2 but for ^{70}Br .

QRPA $_{\beta_2(FRDM)}$				QRPA $_{\beta_2(IBM-1(S))}$				QRPA $_{\beta_2(DD-ME2(O))}$			
E_j	B_{GT}	I	$t_{1/2}^p$	E_j	B_{GT}	I	$t_{1/2}^p$	E_j	B_{GT}	I	$t_{1/2}^p$
1.259	0.279	41.18	2.76E-01	1.258	0.333	36.21	4.63E-01	1.237	0.099	16.95	7.66E-01
1.324	0.024	3.43	3.31E+00	2.329	1.103	62.11	2.70E-01	1.251	0.127	21.58	6.02E-01
2.878	0.022	1.32	8.60E+00					2.722	0.029	2.19	5.94E+00
3.244	0.224	10.94	1.04E+00					2.970	0.027	1.75	7.41E+00
3.338	0.113	5.18	2.19E+00					3.342	0.024	1.25	1.04E+01
3.745	0.030	1.05	1.08E+01					3.431	0.200	9.90	1.31E+00
3.842	0.036	1.20	9.48E+00					3.488	0.128	6.13	2.12E+00
4.719	0.621	10.93	1.04E+00					3.671	0.059	2.50	5.19E+00
5.171	0.451	5.55	2.05E+00					3.997	0.032	1.08	1.21E+01
5.406	0.577	5.81	1.95E+00					4.303	0.091	2.51	5.18E+00
5.683	1.170	9.24	1.23E+00					4.312	0.121	3.30	3.93E+00
								5.018	0.400	6.36	2.04E+00
								5.206	0.577	7.87	1.65E+00
								5.592	1.168	11.44	1.14E+00

QRPA $_{\beta_2(DD-ME2(P))}$				QRPA $_{\beta_2(DD-PC1(O))}$				QRPA $_{\beta_2(DD-PC1(P))}$			
E_j	B_{GT}	I	$t_{1/2}^p$	E_j	B_{GT}	I	$t_{1/2}^p$	E_j	B_{GT}	I	$t_{1/2}^p$
1.398	0.013	1.94	1.30E+01	1.237	0.099	16.95	7.66E-01	1.393	0.012	2.16	1.38E+01
1.785	0.130	15.44	1.63E+00	1.251	0.127	21.58	6.02E-01	1.781	0.129	18.28	1.63E+00
1.785	0.130	15.44	1.63E+00	2.722	0.029	2.19	5.94E+00	1.781	0.129	18.28	1.63E+00
2.089	0.032	3.16	7.94E+00	2.970	0.027	1.75	7.41E+00	2.097	0.032	3.67	8.10E+00
2.101	0.011	1.05	2.38E+01	3.342	0.024	1.25	1.04E+01	2.097	0.011	1.23	2.43E+01
2.245	0.096	8.56	2.93E+00	3.431	0.100	4.95	2.62E+00	2.245	0.098	10.30	2.89E+00
3.223	0.158	7.11	3.53E+00	3.488	0.128	6.13	2.12E+00	3.196	0.162	8.87	3.36E+00
3.492	0.057	2.11	1.19E+01	3.671	0.059	2.50	5.19E+00	3.498	0.060	2.62	1.14E+01
3.492	0.057	2.11	1.19E+01	3.997	0.032	1.08	1.21E+01	3.498	0.060	2.62	1.14E+01
3.656	0.063	2.03	1.23E+01	4.303	0.091	2.51	5.18E+00	3.645	0.062	2.38	1.25E+01
3.734	0.301	9.13	2.75E+00	4.312	0.121	3.30	3.93E+00	3.908	0.045	1.40	2.13E+01
3.734	0.301	9.13	2.75E+00	5.018	0.400	6.36	2.04E+00	3.908	0.045	1.40	2.13E+01
3.991	0.241	5.93	4.24E+00	5.206	0.577	7.87	1.65E+00	3.968	0.248	7.36	4.05E+00
5.279	0.266	1.92	1.31E+01	5.592	1.168	11.44	1.14E+00	5.280	0.266	2.27	1.31E+01
5.283	0.360	2.59	9.70E+00					5.284	0.361	3.07	9.70E+00
5.848	0.322	1.20	2.09E+01					5.851	0.318	1.41	2.12E+01
								5.861	0.306	1.34	2.23E+01
								5.861	0.306	1.34	2.23E+01

Table 5: Same as Table 2 but for ^{70}Kr .

QRPA $_{\beta_2(FRDM)}$				QRPA $_{\beta_2(IBM-1(S))}$				QRPA $_{\beta_2(DD-ME2(O))}$			
E_j	B_{GT}	I	$t_{1/2}^p$	E_j	B_{GT}	I	$t_{1/2}^p$	E_j	B_{GT}	I	$t_{1/2}^p$
0.000	1.016	34.09	1.43E-01	0.004	2.543	49.17	5.71E-02	0.000	1.129	37.60	1.28E-01
0.110	0.439	13.84	3.51E-01	0.663	3.109	40.78	6.88E-02	0.360	0.336	9.10	5.30E-01
0.170	0.049	1.49	3.26E+00	1.873	0.174	1.02	2.74E+00	0.411	0.106	2.79	1.73E+00
0.713	0.530	11.67	4.16E-01	2.918	1.075	2.79	1.01E+00	0.598	0.045	1.06	4.57E+00
1.735	0.225	2.53	1.92E+00	4.336	2.301	1.50	1.87E+00	0.663	0.055	1.24	3.88E+00
1.740	0.197	2.21	2.20E+00	4.622	7.367	3.45	8.14E-01	1.007	0.380	6.91	6.98E-01
1.924	1.045	10.25	4.74E-01					1.100	0.173	2.96	1.63E+00
2.218	0.281	2.22	2.19E+00					1.356	0.149	2.15	2.25E+00
2.264	0.266	2.03	2.39E+00					1.359	0.137	1.97	2.44E+00
2.417	0.283	1.92	2.54E+00					1.593	0.404	4.98	9.69E-01
2.646	0.520	2.94	1.66E+00					1.724	0.167	1.88	2.56E+00
2.869	1.223	5.73	8.48E-01					1.843	0.552	5.70	8.46E-01
								2.127	0.359	3.01	1.60E+00
								2.187	0.137	1.10	4.40E+00
								2.285	0.385	2.87	1.68E+00
								2.699	1.091	5.85	8.25E-01

QRPA $_{\beta_2(DD-ME2(P))}$				QRPA $_{\beta_2(DD-PC1(O))}$				QRPA $_{\beta_2(DD-PC1(P))}$			
E_j	B_{GT}	I	$t_{1/2}^p$	E_j	B_{GT}	I	$t_{1/2}^p$	E_j	B_{GT}	I	$t_{1/2}^p$
0.000	1.382	35.24	1.05E-01	0.000	1.135	37.69	1.28E-01	0.000	1.377	35.68	1.05E-01
0.059	0.132	3.26	1.13E+00	0.376	0.326	8.71	5.52E-01	0.063	0.128	3.20	1.17E+00
0.275	0.286	6.23	5.93E-01	0.427	0.119	3.08	1.56E+00	0.289	0.105	2.30	1.63E+00
0.288	0.106	2.29	1.61E+00	0.597	0.046	1.08	4.45E+00	0.315	0.311	6.73	5.58E-01
0.417	0.168	3.36	1.10E+00	0.651	0.049	1.11	4.33E+00	0.415	0.176	3.58	1.05E+00
0.590	0.177	3.20	1.16E+00	1.022	0.373	6.70	7.18E-01	0.585	0.193	3.56	1.05E+00
0.682	0.474	8.09	4.57E-01	1.118	0.198	3.35	1.44E+00	0.681	0.470	8.16	4.60E-01
0.719	0.334	5.58	6.62E-01	1.325	0.141	2.07	2.32E+00	0.696	0.277	4.76	7.89E-01
0.929	0.573	8.38	4.41E-01	1.328	0.128	1.89	2.55E+00	0.983	0.618	8.88	4.23E-01
1.490	0.222	2.25	1.64E+00	1.502	0.154	2.01	2.39E+00	1.482	0.173	1.79	2.10E+00
2.051	0.550	3.74	9.88E-01	1.543	0.298	3.79	1.27E+00	2.068	0.438	2.99	1.26E+00
2.233	0.488	2.89	1.28E+00	1.675	0.147	1.70	2.82E+00	2.302	0.461	2.64	1.42E+00
2.363	0.286	1.54	2.40E+00	1.832	0.597	6.20	7.76E-01	2.482	0.392	1.95	1.93E+00
2.538	0.458	2.14	1.73E+00	2.102	0.376	3.20	1.50E+00	2.619	0.488	2.17	1.73E+00
4.623	2.316	1.43	2.59E+00	2.253	0.394	3.00	1.61E+00	4.637	3.176	1.95	1.92E+00
				2.682	1.075	5.83	8.26E-01				

Table 6: Same as Table 2 but for ^{72}Kr .

QRPA $_{\beta_2(FRDM)}$				QRPA $_{\beta_2(IBM-1(S))}$				QRPA $_{\beta_2(DD-ME2(O))}$			
E_j	B_{GT}	I	$t_{1/2}^p$	E_j	B_{GT}	I	$t_{1/2}^p$	E_j	B_{GT}	I	$t_{1/2}^p$
0.061	0.022	9.40	1.95E+02	0.270	0.033	18.65	1.62E+02	0.061	0.023	10.09	1.84E+02
0.087	0.014	6.00	3.05E+02	0.774	0.004	1.32	2.28E+03	0.085	0.014	5.86	3.17E+02
0.425	0.007	1.93	9.50E+02	1.143	0.134	23.95	1.26E+02	0.415	0.016	4.67	3.98E+02
0.531	0.016	3.86	4.75E+02	1.418	0.061	7.12	4.24E+02	0.483	0.006	1.69	1.10E+03
0.631	0.028	6.09	3.01E+02	1.535	0.064	6.21	4.86E+02	0.562	0.008	1.87	9.93E+02
0.654	0.029	6.11	3.00E+02	2.175	1.442	42.68	7.07E+01	0.647	0.022	4.73	3.92E+02
0.868	0.011	1.72	1.07E+03					0.747	0.009	1.80	1.03E+03
0.933	0.048	6.96	2.63E+02					0.833	0.012	2.09	8.90E+02
1.030	0.016	1.99	9.19E+02					0.839	0.041	6.87	2.71E+02
1.046	0.011	1.41	1.30E+03					0.855	0.009	1.46	1.27E+03
1.232	0.208	19.74	9.28E+01					0.887	0.026	4.17	4.45E+02
1.261	0.249	22.54	8.13E+01					1.152	0.177	19.15	9.70E+01
1.951	0.045	1.27	1.45E+03					1.215	0.069	6.76	2.75E+02
2.019	0.082	2.00	9.14E+02					1.315	0.149	12.64	1.47E+02
2.070	0.076	1.68	1.09E+03					1.352	0.027	2.12	8.77E+02
								1.510	0.022	1.36	1.36E+03
								1.567	0.021	1.17	1.59E+03
								1.819	0.042	1.53	1.21E+03
								1.933	0.095	2.77	6.70E+02
								2.410	0.130	1.44	1.29E+03
								2.652	0.160	1.02	1.82E+03
QRPA $_{\beta_2(DD-ME2(P))}$				QRPA $_{\beta_2(DD-PC1(O))}$				QRPA $_{\beta_2(DD-PC1(P))}$			
E_j	B_{GT}	I	$t_{1/2}^p$	E_j	B_{GT}	I	$t_{1/2}^p$	E_j	B_{GT}	I	$t_{1/2}^p$
0.106	0.005	2.63	8.42E+02	0.061	0.023	9.69	1.85E+02	0.105	0.005	2.70	8.20E+02
0.200	0.008	3.80	5.83E+02	0.086	0.014	5.70	3.15E+02	0.201	0.008	3.79	5.85E+02
0.263	0.012	4.84	4.58E+02	0.418	0.015	4.13	4.35E+02	0.264	0.012	4.89	4.53E+02
0.395	0.041	14.42	1.54E+02	0.483	0.005	1.36	1.32E+03	0.396	0.041	14.40	1.54E+02
0.885	0.097	18.36	1.21E+02	0.558	0.009	2.07	8.67E+02	0.885	0.096	18.13	1.22E+02
0.986	0.010	1.62	1.37E+03	0.620	0.018	3.84	4.68E+02	0.985	0.009	1.51	1.47E+03
1.153	0.009	1.13	1.97E+03	0.647	0.023	4.81	3.74E+02	1.152	0.008	1.08	2.05E+03
1.158	0.102	13.13	1.69E+02	0.754	0.009	1.56	1.15E+03	1.156	0.098	12.63	1.75E+02
1.410	0.141	12.31	1.80E+02	0.853	0.045	7.26	2.47E+02	1.404	0.147	12.90	1.72E+02
1.418	0.154	13.25	1.67E+02	0.859	0.018	2.91	6.17E+02	1.410	0.157	13.64	1.62E+02
1.857	0.028	1.14	1.94E+03	0.879	0.010	1.55	1.16E+03	1.850	0.031	1.29	1.72E+03
1.919	0.037	1.34	1.66E+03	0.890	0.011	1.73	1.04E+03	1.917	0.037	1.34	1.65E+03
2.081	0.048	1.26	1.76E+03	1.165	0.184	18.95	9.48E+01	2.077	0.048	1.28	1.73E+03
2.084	0.152	3.97	5.59E+02	1.233	0.109	10.15	1.77E+02	2.088	0.151	3.92	5.65E+02
2.255	0.064	1.18	1.89E+03	1.326	0.119	9.56	1.88E+02				
				1.377	0.024	1.77	1.02E+03				
				1.832	0.038	1.31	1.37E+03				
				1.944	0.091	2.54	7.07E+02				
				2.024	0.050	1.19	1.51E+03				
				2.426	0.127	1.31	1.37E+03				

Table 7: Same as Table 2 but for ^{74}Kr .

QRPA $_{\beta_2(FRDM)}$				QRPA $_{\beta_2(IBM-1(S))}$				QRPA $_{\beta_2(DD-ME2(O))}$			
E_j	B_{GT}	I	$t_{1/2}^p$	E_j	B_{GT}	I	$t_{1/2}^p$	E_j	B_{GT}	I	$t_{1/2}^p$
0.077	0.008	5.18	1.48E+04	0.216	0.036	27.40	4.42E+03	0.009	0.003	2.28	3.03E+04
0.199	0.002	1.13	6.78E+04	1.048	0.038	4.25	2.85E+04	0.077	0.019	11.49	6.02E+03
0.220	0.010	5.00	1.54E+04	1.256	0.273	19.47	6.22E+03	0.086	0.013	7.65	9.05E+03
0.262	0.024	10.38	7.39E+03	1.952	2.317	48.35	2.51E+03	0.212	0.037	16.34	4.24E+03
0.321	0.013	5.15	1.49E+04					0.369	0.051	15.94	4.34E+03
0.393	0.005	1.80	4.27E+04					0.652	0.012	1.98	3.50E+04
0.684	0.168	27.65	2.77E+03					0.664	0.016	2.42	2.86E+04
0.869	0.032	3.44	2.23E+04					0.723	0.051	6.93	9.99E+03
0.952	0.233	20.30	3.78E+03					0.844	0.011	1.10	6.31E+04
1.156	0.020	1.09	7.06E+04					0.982	0.016	1.20	5.75E+04
1.416	0.078	2.60	2.95E+04					1.082	0.047	2.75	2.51E+04
1.426	0.051	1.67	4.59E+04					1.139	0.078	4.04	1.71E+04
1.507	0.036	1.03	7.45E+04					1.238	0.048	2.01	3.44E+04
1.561	0.043	1.13	6.81E+04					1.322	0.038	1.38	5.03E+04
1.661	0.094	2.09	3.68E+04					1.377	0.083	2.68	2.59E+04
1.722	0.089	1.80	4.27E+04					1.512	0.085	2.18	3.18E+04
1.822	0.389	6.57	1.17E+04					1.521	0.066	1.66	4.17E+04
								1.580	0.278	6.38	1.09E+04
								2.002	0.302	3.24	2.13E+04
								2.263	0.203	1.14	6.07E+04

QRPA $_{\beta_2(DD-ME2(P))}$				QRPA $_{\beta_2(DD-PC1(O))}$				QRPA $_{\beta_2(DD-PC1(P))}$			
E_j	B_{GT}	I	$t_{1/2}^p$	E_j	B_{GT}	I	$t_{1/2}^p$	E_j	B_{GT}	I	$t_{1/2}^p$
0.086	0.008	5.66	1.55E+04	0.072	0.018	9.76	6.53E+03	0.101	0.007	4.87	1.86E+04
0.169	0.023	13.90	6.31E+03	0.080	0.013	7.19	8.86E+03	0.178	0.023	14.59	6.20E+03
0.174	0.010	6.37	1.38E+04	0.206	0.044	18.38	3.47E+03	0.182	0.011	6.91	1.31E+04
0.555	0.004	1.02	8.63E+04	0.366	0.046	13.25	4.81E+03	0.555	0.024	6.48	1.39E+04
0.632	0.090	19.32	4.54E+03	0.464	0.005	1.27	5.02E+04	0.609	0.019	4.45	2.03E+04
0.714	0.124	21.76	4.03E+03	0.607	0.009	1.51	4.22E+04	0.707	0.146	26.86	3.37E+03
0.878	0.021	2.49	3.53E+04	0.613	0.009	1.51	4.22E+04	0.732	0.006	1.05	8.60E+04
1.119	0.023	1.60	5.48E+04	0.668	0.035	5.01	1.27E+04	0.932	0.047	5.07	1.78E+04
1.125	0.264	17.83	4.92E+03	0.729	0.008	1.03	6.22E+04	1.051	0.048	3.92	2.31E+04
1.715	0.158	3.67	2.39E+04	0.746	0.014	1.63	3.92E+04	1.169	0.270	17.15	5.27E+03
1.854	0.140	2.55	3.44E+04	0.877	0.050	4.29	1.49E+04	1.787	0.222	4.71	1.92E+04
				0.950	0.075	5.43	1.17E+04	1.950	0.127	1.99	4.55E+04
				1.042	0.026	1.56	4.09E+04				
				1.158	0.034	1.57	4.06E+04				
				1.194	0.063	2.70	2.37E+04				
				1.260	0.059	2.21	2.88E+04				
				1.336	0.164	5.29	1.21E+04				
				1.494	0.330	8.04	7.93E+03				
				1.536	0.048	1.09	5.86E+04				
				1.971	0.192	2.03	3.14E+04				
				2.271	0.344	1.74	3.66E+04				

Table 8: Same as Table 2 but for ^{74}Rb .

QRPA $_{\beta_2(FRDM)}$				QRPA $_{\beta_2(IBM-1(S))}$				QRPA $_{\beta_2(DD-ME2(O))}$			
E_j	B_{GT}	I	$t_{1/2}^p$	E_j	B_{GT}	I	$t_{1/2}^p$	E_j	B_{GT}	I	$t_{1/2}^p$
1.002	0.493	41.77	2.92E-01	1.262	0.113	8.43	1.47E+00	2.478	0.541	57.56	3.96E-01
2.480	1.703	58.02	2.11E-01	2.247	2.261	91.57	1.36E-01	3.198	0.573	38.45	5.92E-01
								3.478	0.025	1.37	1.66E+01
								7.368	0.976	1.07	2.12E+01
QRPA $_{\beta_2(DD-ME2(P))}$				QRPA $_{\beta_2(DD-PC1(O))}$				QRPA $_{\beta_2(DD-PC1(P))}$			
E_j	B_{GT}	I	$t_{1/2}^p$	E_j	B_{GT}	I	$t_{1/2}^p$	E_j	B_{GT}	I	$t_{1/2}^p$
1.713	0.717	79.32	3.05E-01	2.559	0.291	47.12	7.72E-01	1.864	0.704	79.30	3.41E-01
2.470	0.042	2.86	8.46E+00	3.146	0.010	1.16	3.13E+01	2.213	0.050	4.53	5.98E+00
3.686	0.617	17.06	1.42E+00	3.187	0.207	22.41	1.62E+00	3.928	0.601	15.22	1.78E+00
				3.187	0.207	22.41	1.62E+00				
				3.214	0.012	1.31	2.79E+01				
				3.214	0.012	1.31	2.79E+01				

Table 9: Same as Table 2 but for ^{74}Sr .

QRPA $_{\beta_2}(\text{FRDM})$				QRPA $_{\beta_2}(\text{IBM-1}(S))$				QRPA $_{\beta_2}(\text{DD-ME2}(O))$			
E_j	B_{GT}	I	$t_{1/2}^p$	E_j	B_{GT}	I	$t_{1/2}^p$	E_j	B_{GT}	I	$t_{1/2}^p$
0.024	0.100	4.47	7.22E-01	0.176	1.099	39.47	7.08E-02	0.040	0.064	3.84	1.14E+00
0.548	0.058	1.98	1.63E+00	1.247	1.593	32.60	8.57E-02	0.490	0.048	2.28	1.91E+00
0.615	0.077	2.56	1.26E+00	1.526	0.463	8.10	3.45E-01	1.029	0.032	1.14	3.82E+00
0.926	0.269	7.57	4.27E-01	2.636	0.809	7.16	3.90E-01	1.099	0.060	2.09	2.09E+00
1.232	0.095	2.27	1.42E+00	2.883	0.786	5.89	4.74E-01	1.257	0.037	1.19	3.68E+00
1.342	0.206	4.61	7.00E-01	4.859	1.719	2.68	1.04E+00	1.411	0.147	4.28	1.02E+00
1.560	0.769	15.24	2.12E-01	6.001	8.068	3.79	7.38E-01	1.524	0.094	2.58	1.69E+00
1.563	0.268	5.31	6.08E-01					1.605	0.114	2.96	1.47E+00
1.779	1.054	18.38	1.76E-01					1.631	0.403	10.35	4.22E-01
1.985	0.199	3.07	1.05E+00					1.778	0.672	15.85	2.75E-01
2.103	0.152	2.19	1.48E+00					1.886	0.050	1.10	3.96E+00
3.148	0.144	1.04	3.12E+00					2.129	0.084	1.61	2.71E+00
3.169	0.611	4.34	7.44E-01					2.153	0.172	3.23	1.35E+00
4.067	0.405	1.46	2.22E+00					2.379	0.141	2.29	1.90E+00
4.268	1.100	3.35	9.64E-01					2.410	0.342	5.46	7.98E-01
4.395	2.931	8.01	4.03E-01					2.568	0.675	9.75	4.47E-01
5.319	1.095	1.26	2.56E+00					2.679	0.361	4.84	9.01E-01
								2.764	1.087	13.79	3.16E-01
								3.858	0.266	1.52	2.86E+00
								5.110	0.853	1.63	2.67E+00

QRPA $_{\beta_2}(\text{DD-ME2}(P))$				QRPA $_{\beta_2}(\text{DD-PC1}(O))$				QRPA $_{\beta_2}(\text{DD-PC1}(P))$			
E_j	B_{GT}	I	$t_{1/2}^p$	E_j	B_{GT}	I	$t_{1/2}^p$	E_j	B_{GT}	I	$t_{1/2}^p$
0.051	0.068	2.72	1.07E+00	0.075	0.216	8.41	3.43E-01	0.060	0.032	1.26	2.31E+00
0.329	0.459	15.90	1.83E-01	0.185	0.049	1.81	1.60E+00	0.261	0.529	18.93	1.53E-01
0.523	0.036	1.14	2.56E+00	0.291	0.239	8.38	3.44E-01	0.597	0.042	1.28	2.27E+00
0.807	0.196	5.32	5.47E-01	0.322	0.498	17.17	1.68E-01	0.796	0.199	5.40	5.38E-01
0.882	0.363	9.44	3.09E-01	0.596	0.056	1.68	1.72E+00	0.895	0.313	8.07	3.60E-01
1.234	0.226	4.87	5.99E-01	0.963	0.106	2.63	1.10E+00	1.233	0.271	5.80	5.01E-01
1.666	1.389	23.35	1.25E-01	0.995	0.243	5.90	4.89E-01	1.673	1.421	23.73	1.22E-01
1.673	0.243	4.07	7.16E-01	1.067	0.301	7.01	4.11E-01	1.875	0.190	2.81	1.03E+00
1.973	0.398	5.57	5.23E-01	1.442	0.140	2.65	1.09E+00	2.055	0.371	4.92	5.90E-01
2.145	0.402	5.07	5.74E-01	1.461	0.138	2.59	1.11E+00	2.264	0.351	4.10	7.09E-01
3.565	0.595	2.86	1.02E+00	1.522	0.183	3.30	8.73E-01	3.664	0.572	2.54	1.14E+00
3.719	0.917	3.92	7.44E-01	1.586	0.113	1.97	1.47E+00	3.679	0.757	3.33	8.73E-01
3.880	0.354	1.33	2.19E+00	2.037	0.194	2.59	1.11E+00	3.835	0.702	2.73	1.06E+00
4.451	0.466	1.10	2.66E+00	2.175	0.329	4.03	7.16E-01	4.385	0.439	1.09	2.67E+00
4.468	1.087	2.52	1.16E+00	2.208	0.818	9.83	2.93E-01	4.542	0.511	1.11	2.63E+00
4.617	0.937	1.90	1.53E+00	2.628	0.131	1.20	2.40E+00	4.705	0.938	1.75	1.66E+00
5.171	0.867	1.04	2.79E+00	2.831	0.246	1.97	1.46E+00	5.181	1.327	1.58	1.84E+00
				3.187	0.539	3.38	8.55E-01				

Table 10: Computed deformation parameters (β_2), total strength (ΣB_{GT}), centroid (\bar{E}), measured and calculated half-lives for $^{68,70}\text{Se}$, ^{70}Br and ^{70}Kr . R_i is a measure of the predictive power of the model and described in Eq. (17).

Nuclei	Decay mode	Q_{β^+} (MeV)	Models	β_2	ΣB_{GT}	\bar{E} (MeV)	$T_{1/2}^{QRPA}$ (s)	$T_{1/2}^{Exp}$ (s)	R_i				
^{68}Se	β^+	4.71	QRPA β_2 (FRDM)	0.23300	3.18	3.43	3.81E+01	3.55E+01 (± 0.7)	1.07				
			QRPA β_2 (NNDC)	0.24200	3.14	3.47	3.97E+01		1.12				
			QRPA β_2 (IBM-1(S))	0.00000	4.10	3.23	1.15E+01		3.09				
			QRPA β_2 (DD-ME2(O))	-0.26900	2.78	3.06	3.08E+01		1.15				
			QRPA β_2 (DD-ME2(P))	0.25100	3.19	3.42	3.45E+01		1.03				
			QRPA β_2 (DD-PC1(O))	-0.27000	2.67	3.04	3.07E+01		1.16				
			QRPA β_2 (DD-PC1(P))	0.25300	3.21	3.42	3.41E+01		1.04				
			^{70}Se	β^+	2.40	QRPA β_2 (FRDM)	-0.30700		1.16	1.24	2.83E+03	2.47E+03 (± 18)	1.15
QRPA β_2 (NNDC)	0.20700	1.05				1.51	3.27E+03	1.33					
QRPA β_2 (IBM-1(S))	0.00000	2.00				1.70	4.52E+03	1.83					
QRPA β_2 (DD-ME2(O))	-0.28100	1.16				1.24	2.75E+03	1.12					
QRPA β_2 (DD-ME2(P))	0.23000	1.21				1.65	3.40E+03	1.38					
QRPA β_2 (DD-PC1(O))	-0.27300	1.15				1.23	2.70E+03	1.10					
QRPA β_2 (DD-PC1(P))	0.23000	1.21				1.65	3.40E+03	1.38					
^{70}Br	β^+	10.50				QRPA β_2 (FRDM)	-0.32700	10.25	7.44	1.14E-01	7.88E-02 (± 0.0003)		3.73
			QRPA β_2 (IBM-1(S))	0.00000	12.77	7.30	1.68E-01	2.13					
			QRPA β_2 (DD-ME2(O))	-0.30800	8.93	7.16	1.30E-01	1.65					
			QRPA β_2 (DD-ME2(P))	0.21400	12.24	7.31	2.51E-01	3.19					
			QRPA β_2 (DD-PC1(O))	-0.30800	8.93	7.16	1.30E-01	1.65					
			QRPA β_2 (DD-PC1(P))	0.21500	11.76	7.46	2.98E-01	3.78					
			^{70}Kr	β^+	9.38	QRPA β_2 (FRDM)	-0.32700	15.49	4.09	4.86E-02		4.50E-02 (± 0.00014)	1.08
						QRPA β_2 (IBM-1(S))	0.00000	16.98	3.06	2.81E-02			1.60
QRPA β_2 (DD-ME2(O))	-0.28800	15.66				4.09	4.82E-02	1.07					
QRPA β_2 (DD-ME2(P))	0.24100	17.76				3.86	3.69E-02	1.22					
QRPA β_2 (DD-PC1(O))	-0.28500	15.67				4.08	4.81E-02	1.07					
QRPA β_2 (DD-PC1(P))	0.24700	17.62				3.84	3.75E-02	1.20					

Table 11: Same as Table 10, but for $^{72,74}\text{Kr}$, ^{74}Rb and ^{74}Sr .

Nuclei	Decay mode	Q_{β^+} (MeV)	Models	β_2	ΣB_{GT}	\bar{E} (MeV)	$T_{1/2}^{pnQRPA}$ (s)	$T_{1/2}^{Exp}$ (s)	R_i				
^{72}Kr	β^+	5.12	QRPA $_{\beta_2}(FRDM)$	-0.36600	2.00	2.60	1.83E+01	1.71E+01 (\pm 0.18)	1.07				
			QRPA $_{\beta_2}(NNDC)$	0.33200	3.37	3.38	2.13E+01		1.25				
			QRPA $_{\beta_2}(IBM-1(S))$	0.00000	2.21	2.56	3.02E+01		1.76				
			QRPA $_{\beta_2}(DD-ME2(O))$	-0.34600	2.14	2.75	1.86E+01		1.09				
			QRPA $_{\beta_2}(DD-ME2(P))$	0.39800	3.38	3.41	2.22E+01		1.30				
			QRPA $_{\beta_2}(DD-PC1(O))$	-0.34900	2.25	2.84	1.80E+01		1.05				
			QRPA $_{\beta_2}(DD-PC1(P))$	0.39700	3.40	3.41	2.21E+01		1.29				
			^{74}Kr	β^+	2.96	QRPA $_{\beta_2}(FRDM)$	0.40100		1.59	1.55	7.67E+02	6.90E+02 (\pm 6.6)	1.11
QRPA $_{\beta_2}(NNDC)$	0.25440	1.66				1.85	8.88E+02	1.29					
QRPA $_{\beta_2}(IBM-1(S))$	0.00000	2.67				1.84	1.21E+03	1.76					
QRPA $_{\beta_2}(DD-ME2(O))$	-0.34200	1.77				1.62	6.92E+02	1.00					
QRPA $_{\beta_2}(DD-ME2(P))$	0.47000	1.30				1.58	8.77E+02	1.27					
QRPA $_{\beta_2}(DD-PC1(O))$	-0.32500	1.89				1.57	6.37E+02	1.08					
QRPA $_{\beta_2}(DD-PC1(P))$	0.48300	1.28				1.58	9.04E+02	1.31					
^{74}Rb	β^+	10.42				QRPA $_{\beta_2}(FRDM)$	0.36600	2.22	2.16	1.22E-01	6.48E-02 (\pm 0.00003)		1.88
			QRPA $_{\beta_2}(IBM-1(S))$	0.00000	2.37	2.20	1.24E-01	1.92					
			QRPA $_{\beta_2}(DD-ME2(O))$	-0.35600	2.49	5.22	2.28E-01	3.52					
			QRPA $_{\beta_2}(DD-ME2(P))$	0.45100	1.39	2.64	2.42E-01	3.73					
			QRPA $_{\beta_2}(DD-PC1(O))$	-0.32500	1.90	5.55	3.64E-01	5.62					
			QRPA $_{\beta_2}(DD-PC1(P))$	0.46300	1.37	2.81	2.71E-01	4.18					
			^{74}Sr	β^+	10.78	QRPA $_{\beta_2}(FRDM)$	0.40100	18.61	4.94	3.23E-02		2.76E-02 (\pm 0.0026)	1.17
						QRPA $_{\beta_2}(IBM-1(S))$	0.00000	18.60	5.64	2.79E-02			1.01
QRPA $_{\beta_2}(DD-ME2(O))$	-0.34700	14.67				5.41	4.36E-02	1.58					
QRPA $_{\beta_2}(DD-ME2(P))$	0.46900	17.06				4.84	2.91E-02	1.06					
QRPA $_{\beta_2}(DD-PC1(O))$	-0.15800	17.13				5.21	2.88E-02	1.05					
QRPA $_{\beta_2}(DD-PC1(P))$	0.48100	16.88				4.88	2.90E-02	1.05					

 Table 12: Predictive power of various pn-QRPA models used in the current investigation. See Eq. (18) for definition of \bar{R} . Only four nuclei were available to calculate the \bar{R} value using QRPA $_{\beta_2}(NNDC)$ because of limited β_2 values from the NNDC database.

Models	\bar{R}
QRPA $_{\beta_2}(FRDM)$	1.53
QRPA $_{\beta_2}(NNDC)$	1.24
QRPA $_{\beta_2}(IBM-1(S))$	1.89
QRPA $_{\beta_2}(DD-ME2(O))$	1.52
QRPA $_{\beta_2}(DD-ME2(P))$	1.77
QRPA $_{\beta_2}(DD-PC1(O))$	1.72
QRPA $_{\beta_2}(DD-PC1(P))$	1.90